Solution Studies of $Ru_2(O_2CR)_4^{n+}$ Complexes ($n = 0, 1$; O_2CR = Octanoate, Crotonate, Dimethylacrylate, Benzoate, *p*-Toluate) and Solid-State Structures of $Ru_2(O_2C$-*p*-tolyl$)_4(THF)_2$, $[Ru_2(O_2C$-*p*-tolyl$)_4(THF)_2]^+[BF_4]^-$, and $Ru_2(O_2C$-*p*-tolyl$)_4(CH_3CN)_2$: Investigations of the Axial Ligation of the Ru_2 Core

Malcolm H. Chisholm,*,† George Christou,† Kirsten Folting,† John C. Huffman,† Chris A. James,‡ John A. Samuels,§ Jodi L. Wesemann,|| and William H. Woodruff‡

Department of Chemistry and Molecular Structure Center, Indiana University, Bloomington, Indiana 47405-4001, and CST-4, Los Alamos National Laboratory, Los Alamos, New Mexico 87545

Received July 7, 1995[⊗]

$Ru_2(O_2C(CH_2)_6CH_3)_4$ (**1a**) is soluble in both coordinating (THF, CH_3OH, CH_3CN) and noncoordinating solvents (benzene, toluene, cyclohexane, CH_2Cl_2), allowing its solution properties to be investigated by ^1H and ^{13}C NMR spectroscopy, UV/visible spectroscopy, resonance Raman spectroscopy, and cyclic voltammetry. In noncoordinating solvents, **1a** exists as an oligomer, presumably by way of axial intermolecular -(- -[Ru_2]- -O- -)$_n$- interactions. ^1H NMR studies of **1a** and $[Ru_2(O_2C(CH_2)_6CH_3)_4]^+[X]^-$**($[1a]^+[X]^-$)**, where X = Cl, BF_4, or $O_2C(CH_2)_6CH_3$, indicate that both dipolar and contact mechanisms contribute to the paramagnetic shifts of the protons. Resonances for axial and equatorial ligands are shifted upfield and downfield, respectively, by a dipolar mechanism. Aromatic ligands in the axial sites, e.g. pyridine and pyrazine, experience an enhanced upfield shift by direct π-delocalization. Comparison of the ^1H NMR signals for $M_2(O_2CR)_4$ compounds where M = Ru and O_2CR = benzoate, toluate, butyrate, crotonate, and dimethylacrylate with those where M = Mo indicates that the equatorial carboxylate ligands in the diruthenium species also experience π-contact shifts. Variable-temperature studies and calculated estimates of dipolar shifts (using structural parameters taken from solid-state structures) indicate a significant zero-field splitting contribution to the dipolar shift. The arrangements of the toluate rings in $Ru_2(O_2C$-*p*-tolyl$)_4(THF)_2$, $Ru_2(O_2C$-*p*-tolyl$)_4(CH_3CN)_2$, and $[Ru_2(O_2C$-*p*-tolyl$)_4(THF)_2]^+[BF_4]^-$ deviate by 15(1), 2.3(2), and 7.3°, respectively, from alignment with the Ru−Ru axis. The Ru−Ru distances for the two neutral and the cationic complexes are 2.27(1) Å, i.e. not significantly affected by the nature of the axial ligand (THF versus CH_3CN) or by charge $n+$ ($n = 0, 1$). The cell parameters for $Ru_2(O_2C$-*p*-tolyl$)_4(THF)_2\cdot 2THF$ at −154 °C are $a = 10.730(5)$ Å, $b = 12.335(6)$ Å, $c = 9.193(4)$ Å, $\alpha = 105.15(2)°$, $\beta = 109.35(2)°$, $\gamma = 77.98(2)°$, $Z = 2$ (asymmetric unit is $RuC_{24}H_{30}O_6$), $d_{calcd} = 1.559$ g/cm^3, and space group $P\bar{1}$. The cell parameters for $Ru_2(O_2C$-*p*-tolyl$)_4(CH_3CN)_2\cdot 3CH_3CN$ at −169 °C are $a = 27.058(3)$ Å, $b = 10.049(1)$ Å, $c = 17.956(2)$ Å, $\beta = 120.89(1)°$, $Z = 4$, $d_{calcd} = 1.465$ g/cm^3, and space group $C2/c$. The cell parameters for $[Ru_2(O_2C$-*p*-tolyl$)_4(THF)_2]^+[BF_4]^-$ at −172 °C are $a = 13.056(4)$ Å, $b = 21.358(6)$ Å, $c = 9.199(2)$ Å, $\beta = 111.28(1)°$, $Z = 2$, $d_{calcd} = 1.350$ g/cm^3, and space group $C2/m$.

Introduction

Dimetal tetracarboxylates, $M_2(O_2CR)_4$, represent an important class of transition metal complexes. For M = Cr,[1] Mo,[2] W,[3] Ru,[4−6] Rh,[7] and Cu,[8] a paddle-wheel or lantern-like structure is adopted in the solid state and each metal is further coordinated along the M−M axis either by a neutral ligand or via intermolecular interactions with its neighbors[9] as shown in **I**.

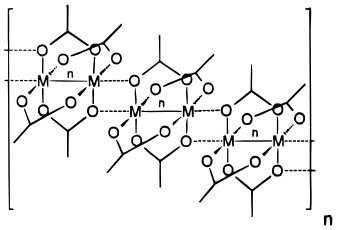

I

Within this series of compounds, the M−M interactions vary from M−M quadruple bonds (M = Cr, Mo, W) to relatively weak antiferromagnetic coupling (M = Cu). For $M_2(O_2CR)_4$ complexes with 4-fold D_{4h} symmetry, the d-orbital splitting

† Indiana University.

‡ Los Alamos National Laboratory.

§ Current address: Watkins-Johnson Co., 440 Kings Village Road, Scotts Valley, CA 95066-4081.

|| Current address: Department of Chemistry, Harvey Mudd College, Claremont, CA 91711.

⊗ Abstract published in *Advance ACS Abstracts,* April 1, 1996.

(1) Cotton, F. A.; Rice, C. E.; Rice, G. W. *J. Am. Chem. Soc.* **1977**, *99*, 4704.

(2) (a) Cotton, F. A.; Daniels, L. M.; Kibala, P. A.; Matusz, M.; Roth, W. J.; Schwotzer, W.; Wang, W.; Zhong, B. *Inorg. Chim. Acta* **1994**, *215*, 9. (b) Martin, D. S.; Hueng, H.-W. *Inorg. Chem.* **1990**, *29*, 3674. (c) Cotton, F. A.; Mester, Z. C.; Webb, T. R. *Acta Crystallogr.* **1974**, *B30*, 2768.

(3) (a) Baxter, D. V.; Cayton, R. H.; Chisholm, M. H.; Huffman, J. C.; Putilina, E. F.; Tagg, S. L.; Wesemann, J. L.; Zwanziger, J. W.; Darrington, F. D. *J. Am. Chem. Soc.* **1994**, *116*, 4551. (b) Chisholm, M. H.; Chiu, H. T.; Huffman, J. C. *Polyhedron* **1984**, *3*, 759.

(4) (a) Bennett, M. J.; Caulton, K. G.; Cotton, F. A. *Inorg. Chem.* **1969**, *8*, 1. (b) Bino, A.; Cotton, F. A.; Felthouse, T. R. *Inorg. Chem.* **1979**, *18*, 2599. (c) Martin, D. S.; Newman, R. A.; Vlasnik, L. M. *Inorg. Chem.* **1980**, *19*, 3404. (d) Drew, M. G. B.; Higgins, P.; McCann, G. M. *J. Chem. Soc., Chem. Commun.* **1987**, 1385. (e) Higgins, P.; McCann, G. M. *J. Chem. Soc., Dalton Trans.* **1988**, 661. (f) Cotton, F. A.; Matusz, M.; Zhong, B. *Inorg. Chem.* **1988**, *27*, 4368. (g) McCann, M.; Carvill, A.; Guinan, P.; Higgins, P.; Campbell, J.; Ryan, H.; Walsh, M. *Polyhedron* **1991**, *10*, 2273. (h) McCann, M.; Carvill, A.; Cardin, C.; Convery, M. *Polyhedron* **1993**, *12*, 1163. (i) Cotton, F. A.; Kim, Y.; Ren, T. *Polyhedron* **1993**, *12*, 607.

S0020-1669(95)00860-3 CCC: $12.00

pattern yields the well-known arrangement of M−M molecular orbitals[10] shown in **II**. This simple pictorial description is

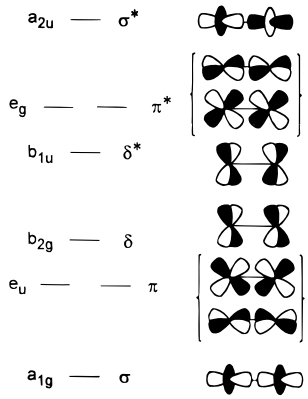

II

pedagogically pleasing but not necessarily accurate since it ignores the mixing of other orbital interactions. For example, for $Mo_2(O_2CR)_4$ and $W_2(O_2CR)_4$ compounds, the M−M σ orbital is not unique because the nd_{z^2} orbital mixes with both the filled (core) np_z orbital and the valence $(n+1)$s orbital. Moreover, the M−M π and δ orbitals can mix with the oxygen p_π orbitals of the bridging carboxylate ligands. The energy separation among σ, π, δ, δ^*, π^*, and σ^* orbitals will also vary with M−M distance, and this in turn will be influenced by the metal, its oxidation state, and the nature of the axial ligands. For M = Cr, the Cr−Cr distance spans a range of ca. 0.4 Å as a function of axial ligation,[11] and the search for an axially free $Cr_2(O_2CR)_4$ compound is an interesting story in itself. Certain workers have argued that $Cr_2(O_2CR)_4$ compounds do not contain M−M quadruple bonds on the basis of calculations,[12] while others have argued against such M−M bonding on the basis of the kinetic lability of the Cr−Cr bond toward rupture in the presence of strongly donating ligands.[13]

The carboxylates of ruthenium,[4−6] $Ru_2(O_2CR)_4^{n+}$ where n = 0 or 1, also have an interesting history with respect to assignment of their electronic structure. The Ru_2^{4+} complexes have two unpaired electrons[5b,5d,14] while those with Ru_2^{5+} cores have three.[4i,15,16] Although the ground state electronic configurations for these carboxylates are now generally accepted to be $\sigma^2\pi^4\delta^2\delta^{*2}\pi^{*2}$ [5d,17,18] and $\sigma^2\pi^4\delta^2\delta^{*1}\pi^{*2}$,[19,20] as shown in **III**, the

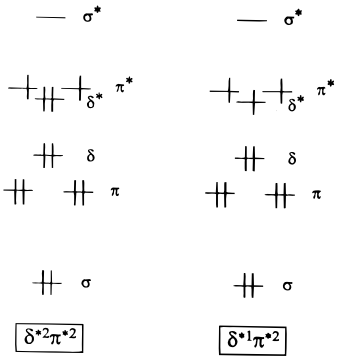

III

ordering of the δ^* and π^* orbitals is not as intuitively obvious as the d-orbital splitting pattern shown in **II** would suggest. Metal−ligand interactions influence their relative energies, and it is apparent that the orbitals must be very close for $Ru_2(O_2CR)_4^{n+}$ where $n = 1$ and are likely to be close for $n = 0$. The usefulness of the simple M−M $\sigma\pi\delta\delta^*\pi^*\sigma^*$ orbital description becomes more limited for these open-shell configurations because of spin−spin and spin−orbit interactions. Although the Ru_2 core has been examined with a variety of bridging ligands in addition to carboxylates to ascertain the effect on electronic structure,[20] no studies have involved systematic variation of the axial ligands of $Ru_2(O_2CR)_4L_2$, nor has anyone determined the ground state of the unligated $Ru_2(O_2CR)_4$. Even the best *ab initio* calculations[17a] that were performed on $Ru_2(O_2CH)_4$ were carried out on a $Ru_2(O_2C)_4$ core with metric parameters taken from $Ru_2(O_2CCH_3)_4(H_2O)_2$. The effect of the axial water molecules of ligation was not considered in terms of its influence on the M−M distance.

In this paper and in the one to follow,[21] we have examined the solution behavior of the hydrocarbon-soluble octanoates of diruthenium with respect to their binding of axial ligands by the use of paramagnetic NMR spectroscopy and other techniques. We have gained insight into the nature of Ru_2−ligand interactions and information pertinent to the molecular design of extended one-dimensional polymers incorporating Ru_4^{4+} centers.

Results and Discussion

The Octanoates. (a) ^{1}H NMR Studies.[22] The ^{1}H NMR spectra of $Ru_2(O_2C(CH_2)_6CH_3)_4$, **1a**, in noncoordinating sol-

(5) (a) Lindsay, A. J.; Wilkinson, G.; Motevalli, M.; Hursthouse, M. B. *J. Chem. Soc., Dalton Trans.* **1987**, 2723. (b) Lindsay, A. J.; Wilkinson, G.; Motevalli, M.; Hursthouse, M. B. *J. Chem. Soc., Dalton Trans.* **1985**, 2321. (c) Lindsay, A. J.; Tooze, P. R.; Motevalli, M.; Hursthouse, M. B.; Wilkinson, G. *J. Chem. Soc., Chem. Commun.* **1984**, 1383. (d) Cotton, F. A.; Miskowski, V. M.; Zhong, B. *J. Am. Chem. Soc.* **1989**, *111*, 6177.
(6) (a) Das, B. K.; Chakravarty, A. R. *Polyhedron* **1991**, *10*, 491. (b) Spohn, M.; Strähle, J.; Hiller, W. *Z. Naturforsch.* **1986**, *41B*, 541.
(7) (a) Cotton, F. A.; Shiu, K.-B. *Rev. Chim. Miner.* **1986**, *23*, 14. (b) Reference 2a.
(8) (a) Campbell, G. C.; Haw, J. F. *Inorg. Chem.* **1988**, *27*, 3706. (b) Lomer, T. R.; Perera, K. *Acta Crystallogr.* **1974**, *B30*, 2912. (c) Lomer, T. R.; Perera, K. *Acta Crystallogr.* **1974**, *B30*, 2913.
(9) $Mo_2(O_2CCPh_3)_4 \cdot 3CH_2Cl_2$ [2a] was shown recently by single-crystal X-ray diffraction to have no axial interactions.
(10) Cotton, F. A.; Walton, R. A. *Multiple Bonds between Metal Atoms*, 2nd ed.; Clarendon Press: Oxford, U.K., 1993; p 18.
(11) Cotton, F. A.; Feng, X.; Kibala, P. A.; Matusz, M. *J. Am. Chem. Soc.* **1988**, *110*, 2807 and references therein.
(12) Hall, M. B. *Polyhedron* **1987**, *6*, 670 and references therein.
(13) Hao, S.; Edema, J. H. H.; Gambarotta, S.; Bensimon, C. *Inorg. Chem.* **1992**, *31*, 2676 and references therein.
(14) (a) Marchon, J.-C.; Maldivi, P.; Giroud-Godquin, A.-M.; Guillon, D.; Skoulios, A.; Strommen, D. P. *Phil. Trans. R. Soc. London A* **1990**, *330*, 109. (b) Maldivi, P.; Giroud-Godquin, A.-M.; Marchon, J.-C.; Guillon, D.; Skoulios, A. *Chem. Phys. Lett.* **1989**, *157*, 552.
(15) (a) Stephenson, T. A.; Wilkinson, G. *J. Inorg. Nucl. Chem.* **1966**, *28*, 2285. (b) Mukaida, M.; Nomura, T.; Ishimori, T. *Bull. Chem. Soc. Jpn.* **1972** , *45*, 2143. (c) Cotton, F. A.; Pedersen, E. *Inorg. Chem.* **1975**, *14*, 388.
(16) Telser, J.; Drago, R. S. *Inorg. Chem.* **1984**, *23*, 3114.
(17) (a) Quelch, G. E.; Hillier, I. H.; Guest, M. F. *J. Chem. Soc., Dalton Trans.* **1990**, 3075. (b) Clark, D. L.; Green, J. C.; Redfern, C. M. *J. Chem. Soc., Dalton Trans.* **1989**, 1037. (c) Clark, D. L.; Green, J. C.; Redfern, C. M.; Quelch, G. E.; Hillier, I. H.; Guest, M. F. *Chem. Phys. Lett.* **1989**, *154*, 326.
(18) Bonnet, L.; Cukiernik, F. D.; Maldivi, P.; Giroud-Godquin, A.-M.; Marchon, J.-C.; Ibn-Elhaj, M.; Guillon, D.; Skoulios, A. *Chem. Mater.* **1994**, *6*, 31.
(19) Norman, J. G., Jr.; Renzoni, G. E.; Case, D. A. *J. Am. Chem. Soc.* **1979**, *101*, 5256.
(20) (a) Cotton, F. A.; Ren, T.; Eglin, J. L. *Inorg. Chem.* **1991**, *30*, 2552. (b) Cotton, F. A.; Ren, T.; Eglin, J. L. *J. Am. Chem. Soc.* **1990**, *112*, 3439. (c) Cotton, F. A.; Feng, X. *Inorg. Chem.* **1989**, *28*, 1180. (d) Cotton, F. A.; Matusz, M. *J. Am. Chem. Soc.* **1988**, *110*, 5761. (e) Chakravarty, A. R.; Cotton, F. A.; Tocher, D. A.; Tocher, J. H. *Polyhedron* **1985**, *4*, 1475.
(21) Wesemann, J. L.; Chisholm, M. H. Submitted.
(22) Historically, paramagnetic NMR data were reported so that the sign of the chemical shift corresponded to the field (upfield shifts were positive). In this report, the current standard convention is used (upfield shifts are negative). The equations stated here correspond to this convention.

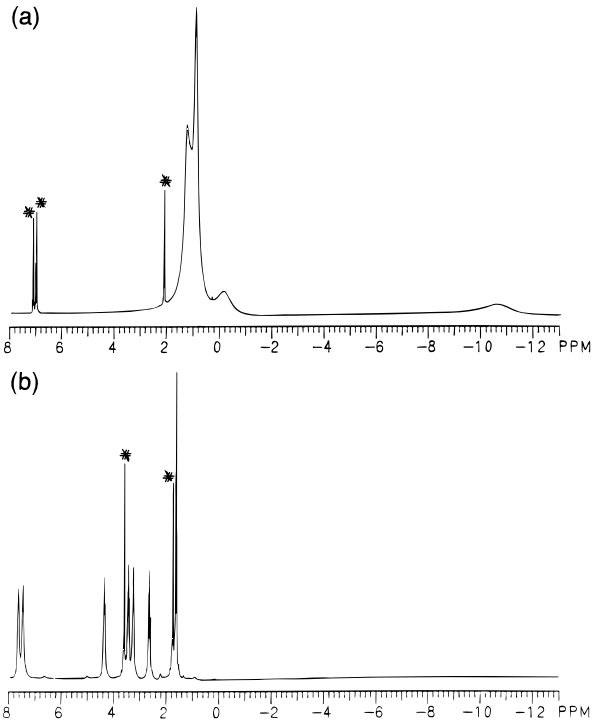

Figure 1. ^{1}H NMR spectra of **1a** in (a) toluene-d_8 and (b) THF-d_8 (asterisk = solvent).

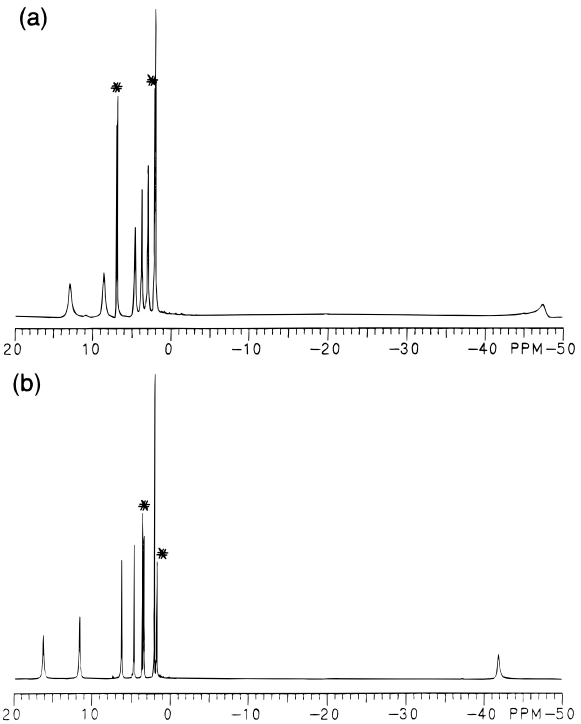

Figure 2. ^{1}H NMR spectra of $[\mathbf{1a}]^+[BF_4]^-$ in (a) toluene-d_8 and (b) THF-d_8 (asterisk = solvent).

vents, such as benzene-d_6, toluene-d_8, dichloromethane-d_2, and cyclohexane-d_{12}, consist of relatively broad and unresolved signals, as shown in Figure 1a. In contrast, the ^{1}H NMR spectra for **1a** in coordinating solvents, such as THF-d_8, methanol-d_4, acetonitrile-d_3, and acetone-d_6, show sharp and well-resolved signals (Figure 1b), more typical of a diamagnetic sample except that the resonances are shifted to lower field. Several explanations were considered to account for the marked difference of the NMR spectral features.

(1) Since compound **1a** is readily oxidized, we were concerned that some oxidation of the Ru_2^{4+} core might have occurred. This, however, was ruled out on two grounds. First, use of Evans' method on samples of **1a** in both coordinating (THF) and noncoordinating (toluene) solvents indicated the presence of two unpaired electrons ($\mu_{eff} \approx 2.8\ \mu_B$), as expected for a Ru_2^{4+} center. The Ru_2^{5+} center has three unpaired electrons. Second, the ^{1}H NMR spectra of cationic complexes $[\mathbf{1a}]^+[X]^-$ in both coordinating and noncoordinating solvents are similar to each other and are readily distinguished from those of **1a**. As shown in Figure 2, the ^{1}H NMR signals for $[\mathbf{1a}]^+[X]^-$ in both types of solvents are fairly well-resolved and span a larger range (−50 to +20 ppm) than those for **1a**.

(2) The possibility that the spectra like those shown in Figure 1a result from the axial ligation of benzene or toluene, which has been seen for certain Cr_2-[11,23] and Rh_2-containing[24] tetracarboxylates, is ruled out by the fact that the same spectral features were observed in dichloromethane-d_2 and cyclohexane-d_{12}. While dichloromethane is known to bind weakly to $Cr_2(OC(CH_3)NR)_4$ complexes,[25] complexation of cyclohexane is unprecedented in these systems.

(3) A change in the electronic ground state could have occurred. For $Ru_2(O_2CR)_4$ complexes where the axial site is occupied with an oxygen atom from either water or neighboring carboxylates magnetic susceptibility measurements show the ground state to be $\delta^{*2}\pi^{*2}$.[5d,18] In the absence of a σ-donor ligand, the energy of the most stable state arising from electronic configuration $\delta^{*1}\pi^{*3}$ might be lower than that from $\delta^{*2}\pi^{*2}$, or at least close enough to be populated to a significant extent at room temperature. Both states are $S = 1$ states and therefore may not be distinguished by Evans' method noted above. The electronic structures of other $Ru_2(bridge)_4$ compounds have been studied,[20] and of these, the triazenido complexes are diamagnetic, having the $\sigma^2\pi^4\delta^2\pi^{*4}$ ground state and an increased Ru−Ru distance.[20d] We would expect that an increased occupation of the Ru_2 π^* orbital in $Ru_2(O_2CR)_4$ would have a marked effect on the Ru−Ru distance. While we were not able to determine the structure of **1a**, we were able to study the effect of various coordinating and noncoordinating solvents on the ν(Ru−Ru) stretching frequency by resonance Raman spectroscopy. (See later.) There is, in general, a relationship between M−M bond length and the value of ν(M−M). However, we observed very little change in ν(Ru−Ru) as a function of solvent and donor ligand and conclude that the further occupation of the π^* orbital and a change in electronic ground state are most unlikely.

(4) Finally, we considered the possibility that **1a** was in fact an oligomer in noncoordinating solvents, existing as a piece of the chainlike structure typically found for unligated $M_2(O_2CR)_4$ compounds in the solid state. (See pictorial description shown in **I**.) Cryoscopic molecular weight determinations were carried out in benzene, and they supported this view. Indeed at ca. 5×10^{-4} M, compound **1a** showed an average degree of association corresponding to a trimer of dinuclear units, i.e. $[Ru_2(O_2C(CH_2)_6CH_3)_4]_3$. The ^{1}H NMR spectra were recorded on more concentrated solutions, which most likely involved an even greater degree of oligomerization. These spectra also showed temperature dependence, the broad signals sharpening with increasing temperature, indicative of dynamic exchange.

For comparison, we examined the ^{1}H NMR spectra of $Rh_2(O_2C(CH_2)_6CH_3)_4$, which is a diamagnetic molecule. It too showed somewhat broad and ill-resolved ^{1}H NMR signals in

(23) Cotton, F. A.; Daniels, L. M.; Kibala, P. A. *Inorg. Chem.* **1992**, *31*, 1865.
(24) Moodley, K. G.; Chisholm, M. H. Unpublished results.
(25) Cotton, F. A.; Ilsley, W. H.; Kaim, W. *J. Am. Chem. Soc.* **1980**, *102*, 3475.

Table 1. ^{1}H NMR Assignments Based on T_1 Values for **1a** and $[\mathbf{1a}]^+[X]^-$

	1a[a]		$[\mathbf{1a}]^+[BF_4]^-$ [a]		$[\mathbf{1a}]^+[O_2C(CH_2)_6CH_3]^+$ [b]			
					equatorial		axial	
	ppm	T_1 (ms)	ppm	T_1 (ms)	ppm	T_1 (ms)	ppm	T_1 (ms)
$CH_2(2)$	3.2	198 ± 1	−42.4	5.5 ± 0.7	−42	11.1 ± 0.3	−27	
$CH_2(3)$	7.4	275 ± 5	16.5	10.2 ± 0.2	11.6	18.7 ± 0.1	−24	7 ± 1
$CH_2(4)$	7.6	344 ± 3	11.8	14.8 ± 0.3	7.3	31.7 ± 0.8	−11.6	19 ± 1
$CH_2(5)$	4.3	702 ± 5	6.3	45.7 ± 0.2	3.9	76.0 ± 1.0	−4.5	45 ± 2
$CH_2(6)$	3.4	958 ± 7	4.7	73.9 ± 0.3	3.2	123.0 ± 1.0	−1.4	87 ± 5
$CH_2(7)$	2.6	1420 ± 20	3.6	122.0 ± 1.0	2.6	173.0 ± 1.0	0.3	154 ± 5
$CH_3(8)$	1.6	1870 ± 10	2.0	223.0 ± 1.0	1.9	236.0 ± 1.0	0.8	251 ± 6

[a] in THF-d_8. [b] In toluene-d_8.

toluene-d_8, which sharpened upon heating. Cryoscopy also indicated that the Rh_2 complex was not monomeric in benzene, and an average n for association was estimated to be 2. For both M = Ru and Rh, it is likely that the degree of association decreases with increasing temperature and the rate of formation and rupture of oligomers by -(- -[M_2]- -O- -)$_n$- interactions increases.

Our conclusion is that the dramatic difference in the appearance of the ^{1}H NMR spectra of **1a** in coordinating and noncoordinating solvents is due to the strong desire of $Ru_2(O_2CR)_4$ molecules to have their axial sites occupied. In coordinating solvents, **1a**$(L)_2$ molecules are present, where L represents an axial ligand provided by the solvent. In noncoordinating solvents, oligomers $[\mathbf{1a}]_n$ form via axial -(- -[M_2]- -O- -)$_n$- interactions. UV/visible, resonance Raman, and cyclic voltammetric data for **1a** in various solvents are consistent with this explanation.

(b) Assignment of the ^{1}H NMR Signals of 1a and $[\mathbf{1a}]^+[X]^-$. Owing to the paramagnetic nature of **1a** and $[\mathbf{1a}]^+[X]^-$, their NMR resonances are shifted from the values seen for the analogous diamagnetic dimolybdenum tetraoctanoate $Mo_2(O_2C(CH_2)_6CH_3)_4$. The shift caused by the unpaired electrons is referred to as the isotropic shift (eq 1)and results

$$\delta_{\text{observed}} = \delta_{\text{diamagnetic}} + \delta_{\text{isotropic}} \quad (1)$$

$$\delta_{\text{isotropic}} = \delta_{\text{dipolar}} + \delta_{\text{contact}} \quad (2)$$

from the distribution of unpaired spin density via dipolar (through-space) and contact (through-bond) mechanisms (eq 2).[26−28] Assignment of the ^{1}H NMR signals and comparison of their isotropic shifts indicate that both dipolar and contact mechanisms occur within the diruthenium tetracarboxylates.

Since the ^{1}H NMR signals for **1a** in THF-d_8 fell in a narrow range, 2-D NMR experiments were used to make assignments. The COSY spectrum is shown in Figure 3. The initial assignment of $CH_3(8)$ was made on the basis of the relative intensity, simple triplet pattern, and chemical shift of the signal at 1.6 ppm. This signal was not significantly different from that of $Rh_2(O_2C(CH_2)_6CH_3)_4$, as would be expected for protons far away from paramagnetic centers. Cross-peaks correlated the CH_2 protons. The basic pattern was an increasing shift in the downfield direction, the protons closer to the metals being more affected. This trend diminished for $CH_2(3)$, whose signal did not shift as far downfield as might be expected, and reversed for $CH_2(2)$, whose signal was shifted back in the upfield direction. T_1 measurements (Table 1) confirmed the COSY assignments, the protons with the shortest T_1 values being closest

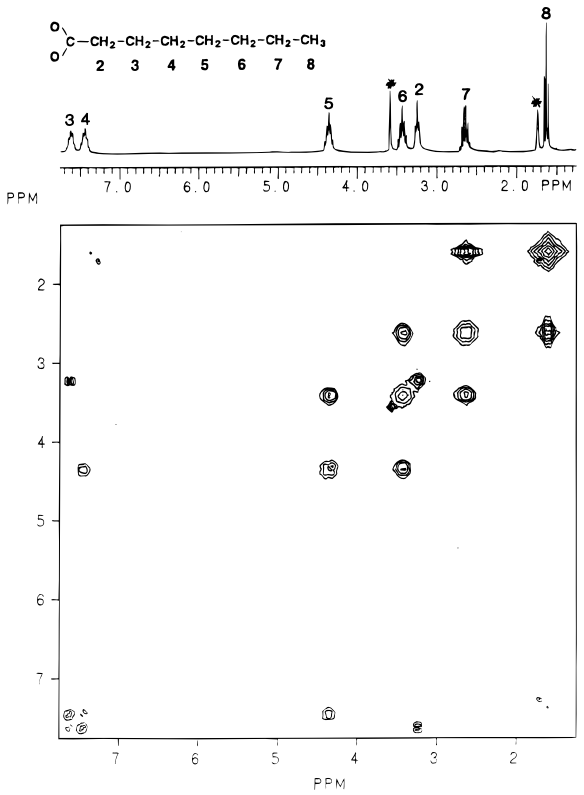

Figure 3. 2-D COSY spectrum for **1a** in THF-d_8.

to the metal−metal bond. T_1 measurements were also used to assign ^{1}H NMR resonances for $[\mathbf{1a}]^+[X]^-$ systems (Figures 2 and 4, Table 1), which possess a third unpaired electron and display similar but exaggerated chemical shift patterns.[29,30] Thus, both dipolar and contact mechanisms appear to contribute to the isotropic shifts of equatorial ligands, one causing downfield and the other causing upfield shifts. More detailed examinations (see below) show that the downfield shifts for the equatorial carboxylate protons in $Ru_2(O_2CR)_4^{n+}$ are due to dipolar (through-space) mechanisms and that the upfield shifts, most obvious for the $CH_2(2)$ protons, may be attributed to contact (through-bond) mechanisms.

The axial ligands of diruthenium tetracarboxyaltes seem to experience both dipolar and contact mechanisms as well. As seen in the ^{1}H NMR spectrum of $[\mathbf{1a}]^+[O_2C(CH_2)_6CH_3]^-$ (Figure 4), the axially-coordinated carboxylate gives rise to a

(26) Satterlee, J. D. *Concepts Magn. Reson.* **1990**, *2*, 69.
(27) Drago, R. S. *Physical Methods in Chemistry*; W. B. Saunders Co.: Philadephia, 1977; Chapter 12.
(28) Drago, R. S.; Zink, J. I.; Richman, R. M.; Perry, W. D. *J. Chem. Educ.* **1974**, *51*, 371, 464.
(29) The chemical shift of $CH_2(2)$ is dependent on the axial ligand. For $[\mathbf{1a}]^+[BF_4]^-$, an upfield signal at −41 ppm was seen in methanol-d_4. For $[\mathbf{1a}]^+[Cl]^+$, in methanol-d_4, which does not completely replace axially-coordinated Cl^-,[30] two signals were seen upfield at −39 and −41 ppm. Addition of NaCl increased the concentration of axially-coordinated Cl^-, indicated by the increased intensity of the signal at −39 ppm.
(30) Drago, R. S.; Cosmano, R.; Telser, J. *Inorg. Chem.* **1984**, *23*, 4514.

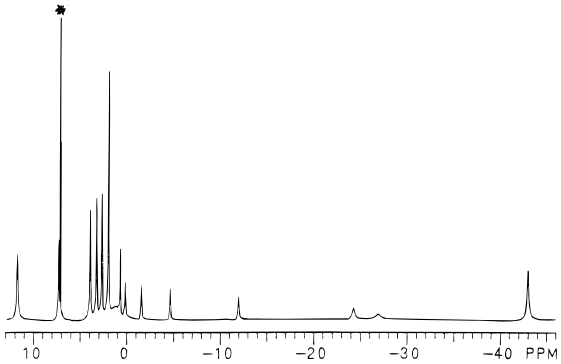

Figure 4. ^{1}H NMR spectra of $[\mathbf{1a}]^+[O_2C(CH_2)_6CH_3]^-$ in benzene-d_6 (asterisk = solvent).

distinct set of signals. Compared to the signals for the equatorial ligands, these signals show a reversed pattern, with signals appearing increasingly upfield for protons closer to the metal center. The $CH_2(2)$ resonance was not shifted as far upfield as might be expected, once again suggesting the occurrence of competing contact mechanisms. Studies on various bis-ligated **1a** and $[\mathbf{1a}]^+[X]^-$ species (see below) show that the upfield shifts for the axial ligands of $Ru_2(O_2CR)_4^{n+}$ are due to dipolar mechanisms (and π-contact mechanisms with aromatic ligands), while the downfield shifts are caused by σ-contact mechanisms.

(c) Dipolar Shifts. The predominantly downfield shift for the equatorial ligands and the shift in the opposite direction for axial ligands suggest that these shifts may be dipolar. Consider the simplified equation for an axially symmetric system,[26,27] given in eq 3.[31] The final term, the geometric factor, shows

$$\delta_{\text{dipolar}} = \frac{-\beta^2 S(S+1)}{9kT}(g_{\parallel}{}^2 - g_{\perp}{}^2)\frac{(1 - 3\cos^2\theta)}{r^3} \qquad (3)$$

the distance and angular dependence of the dipolar shift, r being the distance from the paramagnetic center to the NMR nucleus and θ being the angle relative to the z axis of the molecule. The expression $(1 - 3\cos^2\theta)$ defines a cone ($\theta = 54.7°$) that is aligned along the z axis of the molecule as shown in **IV**.

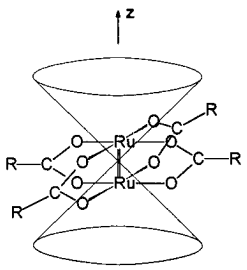

IV

With monomeric axially-symmetric systems, the center of the cone is placed on the paramagnetic metal center. In dinuclear systems where the metal centers are bound directly to each other, the electron density is distributed over the M−M bond and the origin of the cone may be placed in the center of the M−M bond, as in **IV**. Studies on Ru_2^{4+} bis(porphyrin) systems[32] have shown this approach to be more valid than placing a cone at each metal center. The location of a nucleus with respect to the cone will influence its dipolar shift. At the surface of the cone, the geometric factor goes to zero. The equatorial ligands of $Ru_2(O_2CR)_4$ lie outside the cone, where the factor is positive.

(31) As reported in ref 26, the equation predicts the incorrect sign for Fe(III) porphyrin systems (see Supporting Information). The omission of the minus sign has been corrected in the equation reported here.

(32) Collman, J. P.; Barnes, C. E.; Swepston, P. N.; Ibers, J. A. *J. Am. Chem. Soc.* **1984**, *106*, 3500.

Table 2. ^{1}H NMR Resonances (ppm)[a] for Axial Ligands of **1a** and $[\mathbf{1a}]^+$

L		**1a**$(L)_2$	$[\mathbf{1a}(L)_2]^+[BF_4]^-$
pyrazine	*o*-H	−51	−90
2,6-dimethylpyrazine	*o*-H	−1.3	−16
	m-CH_3	−49	−83
pyridine	*o*-H	−47	−89
	m-H	−1.7	−16
	p-H	−33	−45
4-picoline	*o*-H	−47	−73[b]
	m-H	−1.8	−9[b]
	p-CH_3	17	20[b]
THF	2-H	−19	−29
	3-H	−15	−22
2-MeTHF	2-CH_3	−17.8	−32.0[c]
	2-H	−16.8	−33.2[c]
	3/4-H	−14.4	−24.6[c]
		−14.6	−25.5[c]
		−15.2	−29.4[c]
		−15.5	−29.6[c]
	5-H	−18.4	−27.3[c]

[a] At −58 °C except where noted. [b] At −38 °C. [c] Tentative assignments.

Any axial ligands lie inside the cone, where the geometric factor is negative. Thus, the dipolar shifts will be in opposite directions for the equatorial and axial ligands.

Dipolar shifts can be calculated when both g values and structural information are available. Neither are available for the diruthenium tetraoctanoates, but using the g values for other derivatives, the signs of the dipolar shifts can be determined. For $Ru_2(O_2CR)_4$, where $R = (CH_2)_8CH_3$, magnetic susceptibility measurements gave $g_{\parallel} = 1.93$ and $g_{\perp} = 2.22$.[18] For $[Ru_2(O_2CR)_4]^+[Cl]^-$, where $R = (CH_2)_2CH_3$, EPR spectra gave $g_{\parallel} = 1.947$ and $g_{\perp} = 2.200$.[16] Thus, both neutral and cationic diruthenium tetracarboxylate species have negative $(g_{\parallel}{}^2 - g_{\perp}{}^2)$ values. For axial ligands, where θ is less than 54.7°, a negative dipolar (upfield) shift is expected, and for equatorial ligands, a positive (downfield) shift is expected.[22] Since the isotropic shifts seen for **1a** correspond to this, the dipolar mechanism appears to be a major contributor. The ^{1}H NMR signals for the axial ligands (Table 2) are all seen upfield, while the majority of the protons on the equatorial octanoate ligands are shifted downfield. The exception is $CH_2(2)$, whose isotropic shift has significant contact shift contributions.

(d) Contact Shifts. The contact shift depends on bonding interactions, which influence the sign and magnitude of A_{con}, the hyperfine coupling contant for a nucleus and an unpaired electron (eq 4).[26] The effect of an unpaired electron is transmit

$$\delta_{\text{contact}} = \frac{A_{\text{con}}\bar{g}\beta S(S+1)}{3g_n\hbar kT} \qquad (4)$$

ted through molecular orbitals. The transfer may occur via direct delocalization, where unpaired electron density is transferred from the metal orbitals containing the unpaired electrons directly into empty ligand orbitals, or via indirect spin polarization, where unpaired spin density is transferred to fully-occupied metal orbitals and then to ligand orbitals, or both. Both the delocalization and polarization mechanisms may occur through σ and π orbitals. In the $Ru_2(O_2CR)_4^{n+}$ species studied here, π-contributions to the contact shift were expected to dominate since the unpaired electrons occupy π^* (and δ^*, in the case of $[\mathbf{1a}]^+[X]^-$) orbitals. The π-type mechanisms were investigated using aromatic and unsaturated carboxylates and π- and σ-axial ligands, as discussed below. Contributions from σ-polarization mechanisms could occur as well. For the equatorial ligands, such contributions are insignificant. The isotropic shifts of the octanoate ^{13}C NMR signals (Table 3) did not show the

Table 3. ^{13}C NMR Assignments[a] Based on T_1 Values for **1a**

	THF-d_8			toluene-d_8		
	δ_{obs} (ppm)	δ_{iso} (ppm)	T_1 (s)	δ_{obs} (ppm)	δ_{iso} (ppm)	T_1 (s)
C(1)	−92[b]	−277				
C(2)	−72[b]	−110				
C(3)	13.0	−14.7	1.05 ± 0.06	11.3	−16.0	0.37 ± 0.04
C(4)	30.0	−0.1	1.64 ± 0.03	27.3	−2.4	0.66 ± 0.06
C(5)	30.3	0.3	2.81 ± 0.06	29.5	−0.1	1.23 ± 0.02
C(6)	32.4	−0.4	4.14 ± 0.08	32.4	0.0	1.80 ± 0.07
C(7)	22.7	−0.8	5.28 ± 0.14	23.3	0.2	3.00 ± 0.08
C(8)	13.1	−1.2	6.3 ± 0.2	14.4	0.2	4.10 ± 0.07

[a] At 61 °C. [b] Tentative assignments.

alternating pattern typically caused by σ-polarization.[33] Analysis of the chemical shifts for axial ligands (see below) indicates that σ-contact mechanisms are occurring, although π-contributions are larger.

(e) 1/*T* Dependence and Zero-Field Splitting Contributions to the Dipolar Shift. Equations 3 and 4 both predict that the 1/*T* dependence of the chemical shift will be linear and that the observed chemical shift will approach the diamagnetic value as 1/*T* approaches zero. However, deviation from Curie behavior is seen when low-lying states are populated,[34] the hyperfine coupling is temperature dependent,[35] or large zero-field splitting occurs.[36] Of these, the last should be most significant for the diruthenium systems described here.

The effects of zero-field splitting on dipolar shifts are not accounted for in eq 3. In both **1a** and [**1a**]$^+$[X]$^-$, zero-field splitting (ZFS) causes very large D values of ca. 290 cm^{-1} for **1a**[18] and ca. 75 cm^{-1} for [**1a**][X]$^-$.[16] (For mononuclear complexes, D values are usually less than 5 cm^{-1}.[37]) The effect of ZFS on the dipolar shift is included in eq 5 (for $S = 1$) and eq 6 (for $S = {}^3/_2$). The additional terms introduce a $1/T^2$

$$\delta_{dip} = \frac{2\beta^2(g_{||}^2 - g_{\perp}^2)}{9kT}\frac{3\cos^2\theta - 1}{r^3}\left[1 - \frac{g_{||}^2 + {}^1/_2 g_{\perp}^2}{3(g_{||}^2 - g_{\perp}^2)}\frac{D}{kT}\right] \quad (5)$$

$$\delta_{dip} = \frac{5\beta^2(g_{||}^2 - g_{\perp}^2)}{12kT}\frac{3\cos^2\theta - 1}{r^3}\left[1 - \frac{4(g_{||}^2 + {}^1/_2 g_{\perp}^2)}{5(g_{||}^2 - g_{\perp}^2)}\frac{D}{kT}\right] \quad (6)$$

dependence that may be large enough to be seen at lower temperatures if the dipolar contribution dominates the isotropic shift. Since the $(g_{||}^2 - g_{\perp}^2)$ term is negative for $Ru_2(O_2CR)_4^{n+}$, the ZFS contribution will enhance the dipolar shift; i.e., the downfield dipolar shifts seen for the equatorial ligands should be shifted even further downfield at lower temperatures.

The VT ^{1}H NMR data for **1a**, [**1a**]$^+$[BF_4]$^-$, and [**1a**]$^+$[$O_2C(CH_2)_6CH_3$]$^-$ in the range −75 to +40 °C were plotted vs 1/*T* (Figures 5−7). For most signals, the temperature dependence is linear in the measured temperature range. However, for some

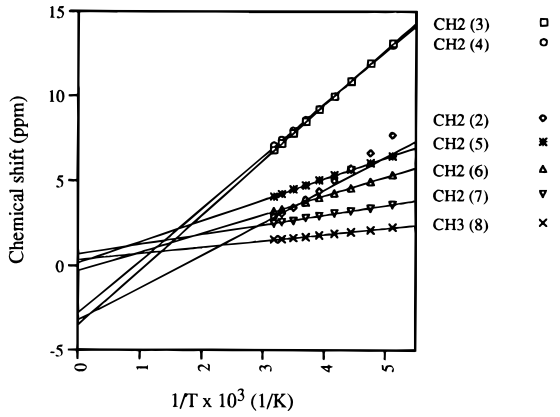

Figure 5. 1/*T* dependence of ^{1}H NMR signals for **1a** in THF-d_8.

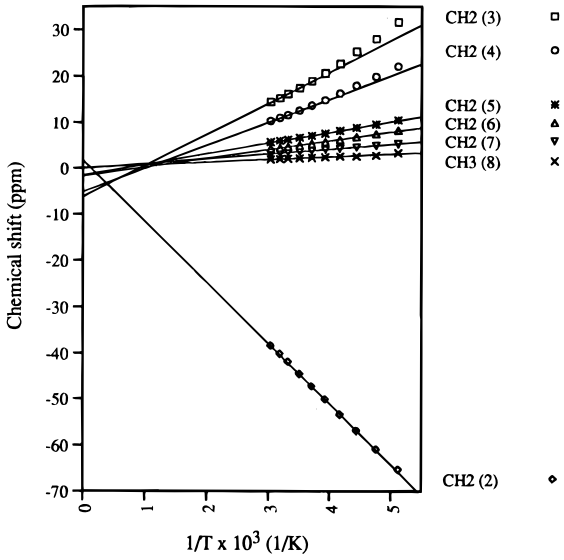

Figure 6. 1/*T* dependence of ^{1}H NMR signals for [**1a**]$^+$[BF_4]$^-$ in THF-d_8.

signals, extrapolation of the data to $1/T = 0$, where both dipolar and contact contributions should become negligible, does not give the chemical shifts one would expect for the diamagnetic species. The protons most affected are the ones closest to the metal−metal bond: CH_2(2), CH_2(3), CH_2(4) for **1a** (Figure 5); CH_2(3), CH_2(4) for [**1a**]$^+$[BF_4]$^-$ (Figure 6) (note that CH_2(2) is dominated by contact shift and thus not affected by ZFS); and CH_2(2), CH_2(3), CH_2(4) for both equatorial and axial carboxylates in [**1a**]$^+$[$O_2C(CH_2)_6CH_3$]$^-$ (Figure 7). Closer examination of some of the data shows nonlinear behavior that can be attributed to $1/T^2$ dependence. Figure 8 shows the data for CH_2(2) of **1a**. Although these protons have a large contact contribution (which causes the resonance to be shifted upfield relative to the others), the dipolar contribution is also expected to be strong due to the proximity of the protons to the metal−metal bond. In contrast, for [**1a**]$^+$[BF_4]$^-$ the CH_2(2) data are linear. Here, the presence of an extra unpaired electron is expected to increase both dipolar and contact contributions due to the $S(S + 1)$ factor in eqs 3 and 4. However, the cationic species have lower D values, which should decrease the dipolar contribution due to ZFS, and shorter Ru−O bonds, which should increase the through-bond contact interaction. Thus, CH_2(2) is dominated by contact shift, causing linearity in 1/*T* and an intercept at $1/T = 0$, which corresponds to diamagnetic values. For CH_2(3) and CH_2(4), the relative dipolar contribution is larger, causing nonlinear behavior (Figure 9) and a negative chemical shift value at $1/T = 0$. For [**1a**]$^+$[$O_2C(CH_2)_6CH_3$]$^-$,

(33) Morishima, I.; Okada, K.; Yonezawa, T.; Goto, K. *J. Am. Chem. Soc.* **1971**, *93*, 3922.
(34) (a) La Mar, G. N.; Eaton, G. R.; Holm, R. H.; Walker, F. A. *J. Am. Chem. Soc.* **1973**, *95*, 63. (b) Bertini, I.; Luchinat, C.; Messori, L.; Vašák, M. *J. Am. Chem. Soc.* **1989**, *111*, 7300. (c) Banci, L.; Bertini, I.; Briganti, F.; Luchinat, C. *New J. Chem.* **1991**, *15*, 467.
(35) (a) Wüthrich, K. *Struct. Bonding* **1970**, *8*, 53. (b) Horrocks, W. DeW., Jr.; Greenberg, E. S. *Mol. Phys.* **1974**, *27*, 993.
(36) (a) Chmielewski, P. J.; Latos-Grażyński, L. *Inorg. Chem.* **1992**, *31*, 5231. (b) Latos-Grażyński, L. *Inorg. Chem.* **1985**, *24*, 1681. (c) Reference 34a. (d) Behere, D. V.; Birdy, R.; Mitra, S. *Inorg. Chem.* **1982**, *21*, 386.
(37) Kurland, R. J.; McGarvey, B. R. *J. Magn. Reson.* **1970**, *2*, 286. Please note that the signs of the equations taken from this article have been switched to correspond to the convention used here.

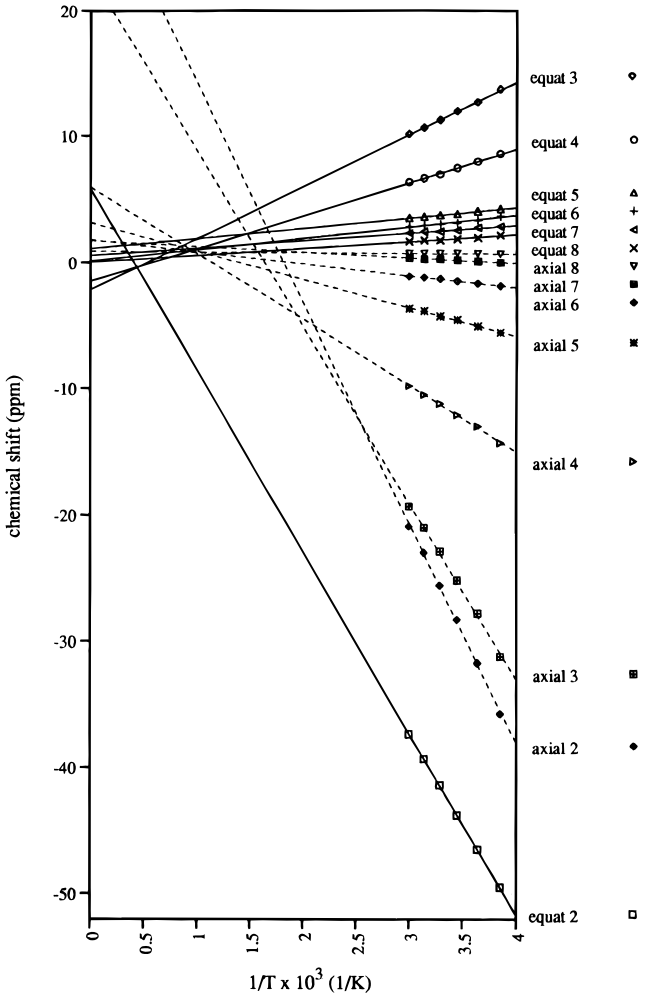

Figure 7. $1/T$ dependence of ^{1}H NMR signals for $[\mathbf{1a}]^+[O_2C(CH_2)_6CH_3]^-$ in toluene-d_8.

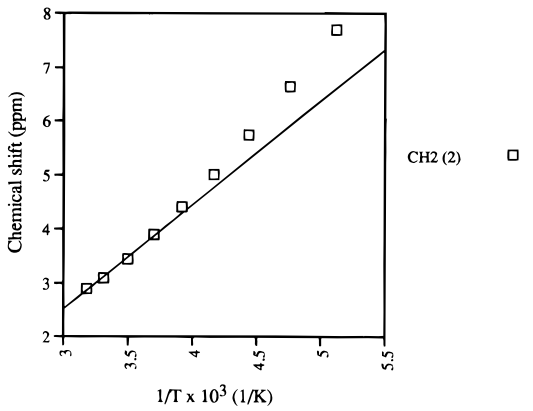

Figure 8. Non-Curie behavior of $CH_2(2)$ of **1a**.

the curvature of the lines is not as apparent, but only six data points were taken over a smaller temperature range.

(f) Axial Ligands. Addition of axial ligands to **1a** in toluene-d_8 results in an equilibrium between $\mathbf{1a}(L)_2$ and $[\mathbf{1a}]_n$ (eq 7).

$$[\mathbf{1a}]_n + 2L \rightleftharpoons \mathbf{1a}(L)_2 \qquad (7)$$

For L = pyridine and pyrazine, which coordinate more strongly than nitriles and THF, the equilibrium lies to the right, as indicated by room-temperature ^{1}H NMR spectra which show the resolved signals of an axially-coordinated species. For L = THF and benzonitrile, resolved signals are seen only at low temperature. At room temperature, the broad signals indicative of $[\mathbf{1a}]_n$ are seen.

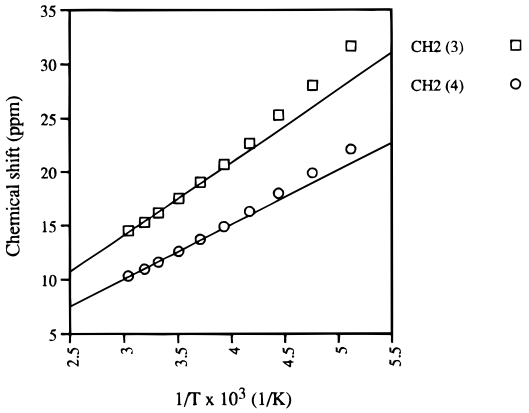

Figure 9. Non-Curie behavior of $CH_2(3)$ and $CH_2(4)$ of $[\mathbf{1a}]^+[BF_4]^-$. ^{1}H NMR signals of $CH_2(2)$ vary linearly with $1/T$, presumably due to large contact contributions.

Axial ligand exchange also occurs when more than 2 equiv is present, preventing signals for the axially-coordinated ligands from being detected at room temperature. When the sample was cooled, the exchange process was slowed. The appearance of free and axially-coordinated ligands was generally seen by −18 °C, except for THF and benzonitrile, which needed to be cooled to −45 and −65 °C, respectively, suggesting that these ligands are not as strongly bound as the nitrogen heterocycles.

Consistent with our earlier analysis, all the ^{1}H NMR resonances for axial ligands of $\mathbf{1a}(L)_2$ and $[\mathbf{1a}(L)_2]^+[X]^-$ (Table 2) are shifted upfield due to the dipolar contributions expected for protons in close proximity to paramagnetic centers. A closer look at the overall shift patterns indicates that π-contact contributions are also occurring. The shifts for the ligands containing π-systems (pyrazines and pyridines) are significantly further upfield than for those without (THF).[38] The effect seen for methyl substitution in the ligands with π-systems, where the CH_3 resonance is paramagnetically shifted in the direction opposite to the H it replaced, also indicates that the contact contribution is due to π-interactions.[27] Substitution of the 2-position in THF with a methyl group showed no such shifts for **1a** and only slightly upfield shifts for $[\mathbf{1a}]^+[X]^-$, confirming that no major π-contribution is occurring via a polarization mechanism.

Further examination of the shift patterns indicates that direct π-delocalization of the unpaired electrons occupying the Ru−Ru π^* orbital into the aromatic π-system of the axial pyrazine and pyridine ligands is occurring. A nonattenuating upfield, downfield, upfield shift pattern for the *ortho*-, *meta*- and *para*-positions on an aromatic ring is indicative of π-delocalization.[38] If the upfield dipolar shifts for the axial ligands pyrazine and pyridine are disregarded, such a pattern is seen. On the basis of similar chemical shift values, π-delocalizations are occurring to the same degree in both ligands.

(g) ^{1}H NMR Spectra of $[\mathbf{1a}]_n$. In regard to the above discussion, the broad signals seen for **1a** in noncoordinating solvents can be explained. Half of the carboxylate ligands in the oligomeric species are involved with intermolecular -(- -$[M_2]$- -O- -)$_n$- interactions. These ligands are axial to one Ru_2^{4+} unit, as well as equatorial to another, resulting in the upfield axial shifts being counteracted by the downfield equatorial shifts. Since the oligomer is dynamic, breaking and reforming M- -O bonds either by rotation or by complete dissociation and association, exchange of the carboxylates in

(38) Horrocks, W. DeW., Jr. In *NMR of Paramagnetic Molecules: Principles and Applications*; La Mar, G. N., Horrocks, W. DeW., Holm, R. H., Eds.; Academic Press: New York, 1973; Chapter 4.

Table 4. Solvent Dependence of Electronic Spectra of **1a**

solvent	λ_{max} (nm)	λ_{max} (cm^{-1})	ϵ (M^{-1} cm^{-1})
toluene	460	21 740	1100
benzene	462	21 650	1200
dichloromethane	454	22 030	710
acetonitrile	458	21 840	830
1:2 benzene/pyrazine	475	21 060	3000
1:2 benzene/pyridine	442 (sh)	22 620	1490
	406	24 630	1800
THF	438	22 840	970
methanol	438	22 840	720

the axial site results in only one set of broadened signals. The butyrate derivative shows a very similar spectrum in noncoordinating solvents. Thus the broad signal at −10 ppm is assigned to CH_2(2), while the signals for the remaining equatorial protons fall between −1 and +2 ppm.

(h) UV−Visible Spectroscopic Studies. The solvent-dependent electronic absorption data for **1a** in the visible region are given in Table 4. The characteristic absorption seen at ca. 460 nm ($\epsilon \approx 1100-1200$ M^{-1} cm^{-1}) in benzene and toluene solutions shifts to slightly higher energy with a change to oxygen-donor solvents, e.g. 438 nm in methanol and THF ($\epsilon \approx$ 720 and 970 M^{-1} cm^{-1}, respectively). In the presence of pyrazine, there is a small but distinct red shift to 475 nm and, perhaps more significantly, the molar absorptivity increases to $\epsilon \approx 3000$ M^{-1} cm^{-1}. With pyridine (2 equiv) the axially-ligated complex **1a**$(py)_2$ shows a splitting of this absorption, namely λ_{max} at 406 nm ($\epsilon \approx 1800$ M^{-1} cm^{-1}) and a shoulder at 442 nm ($\epsilon \approx 1490$ M^{-1} cm^{-1}).

An unequivocal assignment of this band has never been made for Ru_2^{4+} tetracarboxylates. The molar absorptivity is consistent with a primarily M−M d-based electronic transition. In the symmetry point group D_{4h}, assuming the $^3A_{2g}$ ground state of $\delta^{*2}\pi^{*2}$, the Ru_2^{4+} $\pi \rightarrow \pi^*$ ($e_u \rightarrow e_g$) transition is allowed in the *z* direction. We believe the band observed at ca. 460 nm corresponds to this transition. Single-crystal polarization studies in the UV/visible region showed that the $\pi \rightarrow \pi^*$ transition for the cationic Ru_2^{5+} species $Ru_2(O_2CCH_3)_4Cl$ occurs at 460 nm ($\epsilon \approx 1000$ M^{-1} cm^{-1}),[39] in good agreement with our assumption. Other possible assignments for the band seem unlikely. Of the $\delta/\delta^* \rightarrow \pi^*$ transitions, only $\delta^* \rightarrow \pi^*$ ($b_{1u} \rightarrow e_g$) is allowed by symmetry (*x*,*y*). Given the anticipated proximity of these orbitals, the energy of the observed transition (ca. 460 nm) seems too high for a $\delta^* \rightarrow \pi^*$ transition. The $\delta^* \rightarrow \pi^*$ transition for the cationic Ru_2^{5+} core has been seen at ca. 1450 nm (6900 M^{-1} cm^{-1}) in the near-IR spectrum in single-crystal polarization studies.[40] For the neutral compound **1a**, we saw no evidence of a near-IR band; however, our data were obtained in solution. The $\pi/\pi^* \rightarrow O_2C$ π^* transitions, being MLCT transitions, are also unlikely assignments for this absorption of relatively low intensity. For $M_2(O_2CR)_4$ compounds where M = Mo and W, the $\delta \rightarrow O_2C$ π^* transitions have molar absorptivities of approximately 13 000 M^{-1} cm^{-1}.[41] Since these absorptions are at least 10 times as intense as the band seen for **1a**, we feel comfortable in suggesting that the band at ca. 460 nm is indeed due to the $\pi \rightarrow \pi^*$ transition.

On the basis of this assignment, the shift in the electronic spectra and changes in molar absorptivity with different axial ligands must be due to π-interactions either with the Ru−Ru π^* or Ru−Ru π orbitals. The π LUMOs of pyrazine, pyridine,

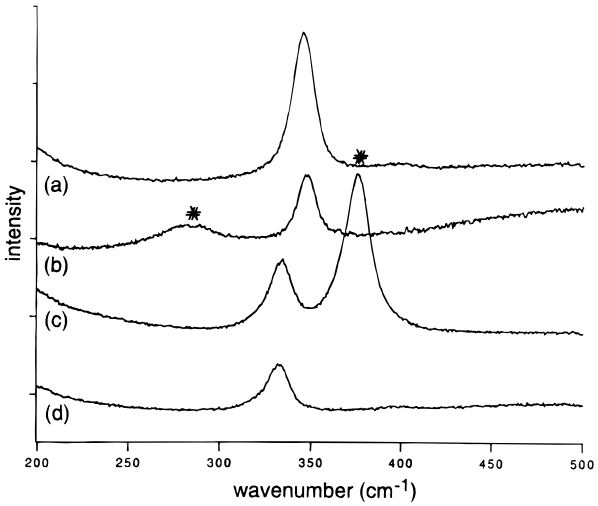

Figure 10. Solution resonance Raman spectra of **1a** showing the Ru−Ru stretch in (a) benzene, (b) THF, (c) acetonitrile, and (d) benzene with 2 equiv of pyridine (asterisk = solvent).

Table 5. Solvent Dependence of the Ru−Ru Stretch of **1a** in the Resonance Raman Spectra

solvent	ν(Ru−Ru) (cm^{-1})	solvent	ν(Ru−Ru) (cm^{-1})
benzene	348	acetonitrile	335
THF	347	1:2 benzene/pyridine	332

and acetonitrile are of correct symmetry to interact with the Ru−Ru π^* HOMO, lowering the π^* orbital in energy, resulting in a lower energy $\pi \rightarrow \pi^*$ transition, and increasing the ligand character of the π^* orbtial, resulting in a more allowed transition. This effect is most prominent for **1a**$(pz)_2$. Extended Hückel molecular orbital calculations show that the pyrazine LUMO, which is less than 1 eV higher in energy, does stabilize the Ru−Ru π^* orbital,[21] supporting this conclusion. Although the filled p orbitals of halides have been shown to interact with Ru−Ru π orbitals, increasing their energies and also decreasing the energies of the $\pi \rightarrow \pi^*$ transitions for $[Ru_2(O_2C(CH_2)_2CH_3)_4]^+[X]^-$,[39] the ligands investigated here are not expected to have any significant interactions with the Ru−Ru π orbital. Methanol and THF, whose π lone pairs are directed away from the metal centers, are primarily σ-donors. The filled π orbitals of acetonitrile, pyridine, and pyrazine will lie at energies much lower than that of the Ru−Ru π^* orbital, precluding strong interactions. Since the absorbances and molar absorptivities for $[\mathbf{1a}]_n$ fall between those seen for **1a**$(L)_2$ with π-acceptor and non-π-acceptor ligands, we conclude that the axial carboxylates are also forming π-interactions with the Ru−Ru π^* orbtials, although to a lesser degree.

(i) Resonance Raman Spectroscopy. On the basis of the evidence for axial π-interactions in the visible spectra, we expected corresponding shifts in the Ru−Ru stretch, a transfer of Ru−Ru π^* electrons to ligand π systems strengthening the Ru−Ru bond. Although the Ru−Ru stretch seen in resonance Raman spectra was affected by solvent (Figure 10, Table 5), the stretches for **1a**$(L)_2$ were lower for L = pyridine and acetonitrile (332 and 335 cm^{-1} respectively) than for L = THF (347 cm^{-1}). Also $[\mathbf{1a}]_n$ in benzene had a Ru−Ru stretch of 348 cm^{-1}. The similarity of this stretch to that of **1a**$(THF)_2$, which has an axial Ru−O bond, supports the presence of axial $-(-[M_2]-O-)_n-$ interactions within $[\mathbf{1a}]_n$.

The strength of the Ru−Ru bond is apparently affected much more by σ-interactions than π-interactions. This corresponds

(39) Miskowski, V. M.; Gray, H. B. *Inorg. Chem.* **1988**, *27*, 2501.
(40) Miskowski, V. M.; Loehr, T. M.; Gray, H. B. *Inorg. Chem.* **1987**, *26*, 1098.
(41) Chisholm, M. H.; Clark, D. L.; Huffman, J. C.; Van Der Sluys, W. G.; Kober, E. M.; Lichtenberger, D. L.; Bursten, B. E. *J. Am. Chem. Soc.* **1987**, *109*, 6796.
(42) Ketteringham, A. P.; Oldham, C. *J. Chem. Soc., Dalton Trans.* **1973**, 1067.

Table 6. Cyclic Voltammetry of $M_2(O_2C(CH_2)_6CH_3)_4$ (M = Ru, Rh, Mo)[a,b]

	$E_{1/2}(M_2^{4+}/M_2^{5+})$ (mV)				
	CH_2Cl_2	(CH_2Cl_2 − CH_3CN)	CH_3CN	(CH_3CN − THF)	THF
Ru	−233	(59)	−292	(77)	−369
Rh	820	(84)	726		
Mo	152	(166)	−14	(66)	−80

[a] Electrolyte solutions contained 0.1 M $^nBu_4NPF_6$. [b] All $E_{1/2}$ values referenced to the ferrocene/ferrocenium couple in the appropriate solvent.

to Raman studies done on $Rh_2(O_2CCH_3)_4$,[42] which showed that the Rh−Rh stretch is influenced by axial interactions with the σ^* orbital, decreasing with increasing donor strength. Unfortunately, nitrogen ligands were not included in this study, and thus, direct comparisons cannot be made to our results. For **1a** in oxygen-donor and noncoordinating solvents, where carboxylate oxygens are presumed to occupy the axial site, the Ru−Ru stretch was 348 cm^{-1}. In the presence of nitrogen-donors, the stretch was lowered to 335 cm^{-1}. Similar behavior was seen for $Mo_2(O_2C(CH_2)_6CH_3)_4$ (405 cm^{-1} in THF, 397 cm^{-1} in acetonitrile).

Contrary to what one might expect, the Ru−Ru stretches in the neutral species, with bond orders of 2, were slightly higher than those previously measured for the cationic species, with bond orders of 2.5. In the solid state, Ru−Ru stretches reported for $Ru_2(O_2CR)_4Cl$ (R = H, CH_3, C_2H_5, C_3H_7) range from 326 to 331 cm^{-1}.[43] In ethanol, where the axial chlorides are replaced by solvent, $Ru_2(O_2CC_3H_7)_4^+$ has a Ru−Ru stretch of 341 cm^{-1}.[43a] The similar stretches of $Ru_2(O_2CR)_4$ and $Ru_2(O_2CR)_4^+$ species support the ground state configuration of $\delta^{*2}\pi^{*2}$ for the former. The $\delta^{*1}\pi^{*3}$ state, with increased occupation of the π^* orbital, would lead to a lower value for ν(Ru−Ru).

(j) Electrochemical Studies. The effect of the solvent, donor vs nondonor, on the **1a**/[**1a**]$^+$ redox couple reflects the energy of the HOMO of **1a** as a function of axial ligation. It is, of course, also a measure of the relative stability of the cationic species and its solvation. In order to separate these two factors, or at least evaluate them in a comparative fashion, we measured the corresponding redox couple for $Mo_2(O_2C(CH_2)_6CH_3)_4$ in the same solvents. We also attempted to obtain the data for $Rh_2(O_2C(CH_2)_6CH_3)_4$ and its cation, but due to its high redox potential, we were limited to CH_2Cl_2 and CH_3CN as solvents. The data are collected in Table 6. The first point to note from the data is that the ease of oxidation of $M_2(O_2C(CH_2)_6CH_3)_4$ compounds follows the order M = Ru > Mo > Rh. Since these are all second-row transition elements, this is a good indication of the M−M HOMO energy. Thus, it is easier to oxidize the Ru_2^{4+} complexes with the M−M electronic configuration $\sigma^2\pi^4\delta^2\delta^{*2}\pi^{*2}$ (where electrons occupy higher energy antibonding orbitals) relative to the Mo_2^{4+} complexes with the M−M configuration $\sigma^2\pi^4\delta^2$. The large difference between the oxidation potentials of the Ru_2 and Rh_2 complexes is most striking, especially since the M−M HOMO for each is π^{*2} and π^{*4}, respectively. We suggest that three factors are responsible for this: (1) Rh is more electronegative than Ru.[44] (2) Oxidation of the Ru_2^{4+} core yields Ru_2^{5+} with three unpaired electrons whereas the related oxidation of the Rh_2^{4+} center yields only one unpaired electron.[45] Thus, the former is stabilized to a maximum degree by Hund's rule, which favors a ground state having the highest spin multiplicity. (3) It is known that, with strong axial ligands, the $Rh_2(O_2CR)_4^+$ has a HOMO with one unpaired electron in a M−M orbital of σ character.[46] Thus, the simple d-orbital splitting pattern shown in **II** is beginning to break down for the d^7−d^7 tetracarboxylates of rhodium.

The data in Table 6 also show the influence of solvent. The trend THF > CH_3CN > CH_2Cl_2 indicates that the ease of oxidation increases with the ability of the solvent to stabilize the cation. An interesting comparison emerges between the M_2^{4+}/M_2^{5+} couples (M = Ru, Mo) in the solvents CH_2Cl_2 and CH_3CN. The influence of solvent change for M = Ru is modest (59 mV) compared to that for M = Mo (166 mV). This we believe is due to the fact that $Ru_2(O_2C(CH_2)_6CH_3)_4$ is in fact an oligomer in CH_2Cl_2 (as noted earlier), whereas the Mo_2^{4+} carboxylate binds axial ligands much more weakly. (This matter has been discussed in terms of the temperature range of the mesophases for the $M_2(O_2C(CH_2)_6CH_3)_4$ compounds.[3a])

The Arenecarboxylates. In the case of $Mo_2(O_2CAr)_4$ complexes, there is a significant interaction between the M−M δ HOMO and the aromatic ring via the O_2C π system. This interaction occurs due to the favored coplanar arrangement for the O_2CR and aromatic π systems and manifests itself in a strong red shift in the $\delta \rightarrow O_2C$ π^* MLCT absorption.[47] In the case of $Ru_2(O_2CAr)_4$, charge transfer bands involving the carboxylates are not seen. Thus, in order to investigate the interactions between the Ru_2^{n+} (n = 4, 5) core and the aromatic rings, we have carried out certain structural studies along with an investigation of the way in which the paramagnetic Ru_2^{n+} (n = 4, 5) cores influence the ^1H NMR signals within the aromatic ring.

The ^1H NMR data for the arenecarboxylates, as discussed below, indicate that unpaired spin density is being transferred to the aromatic π orbitals. These studies were meant to determine which molecular orbitals and, thus, which contact mechanisms might be responsible for the isotropic shifts of the equatorial carboxylates. A direct π-delocalization mechanism would involve transfer from the π^* orbtial as shown in **V**. For

V **VI**

the aromatic π system to overlap with the carboxylate orbital, the ring would need to be perpendicular to the plane of the carboxylate. A π-polarization mechanism would involve the planar O_2C−aromatic ring arrangement seen for $Mo_2(O_2CAr)_4$ but would require that the unpaired electrons be polarizing the

(43) (a) Clark, R. J. H.; Franks, M. L. *J. Chem. Soc., Dalton Trans.* **1976**, 1825. (b) Clark, R. J. H.; Ferris, L. T. H. *Inorg. Chem.* **1981**, *20*, 2759. (c) Miskowski, V. M.; Loehr, T. M.; Gray, H. B. *Inorg. Chem.* **1988**, *27*, 4708.

(44) Pauling electronegativities: Rh, 2.28; Ru, 2.2; Mo(II), 2.16. From: Huheey, J. E.; Keiter, E. A.; Keiter, R. L. *Inorganic Chemistry: Principles of Structure and Reactivity*, 4th ed.; Harper Collins: New York, 1993.

(45) Kawamura, T.; Katayama, H.; Nishikawa, H.; Yamabe, T. *J. Am. Chem. Soc.* **1989**, *111*, 8156.

(46) (a) Drago, R. S.; Cosmano, R.; Telser, J. *Inorg. Chem.* **1984**, *23*, 3120. (b) Kawamura, T.; Fukamachi, K.; Sowa, T.; Hayashida, S.; Yonezawa, T. *J. Am. Chem. Soc.* **1981**, *103*, 364. (c) Kawamura, T.; Fukamachi, K.; Hayashida, S. *J. Chem. Soc., Chem. Commun.* **1979**, 945.

(47) San Filippo, J., Jr.; Sniadoch, H. J. *Inorg. Chem.* **1976**, *15*, 2209.

(48) (a) M = Cr, R = Ph, ∠ = 6.0°: Cotton, F. A.; Extine, M. W.; Rice, G. W. *Inorg. Chem.* **1978**, *17*, 176. (b) M = Mo, R = Ph, ∠ = 7.2°: Collins, D. M.; Cotton, F. A.; Murillo, C. A. *Inorg. Chem.* **1976**, *15*, 2950. (c) M = W, R = Ph, ∠ = 10.7°: Cotton, F. A.; Wang, W. *Inorg. Chem.* **1984**, *23*, 1604. (d) M = Co, R = Ph, ∠ = 5.9°: Davies, J. E.; Rivera, A. V.; Sheldrick, G. M. *Acta Crystallogr.* **1977**, *B33*, 156. (e) M = Rh, R = Ph, ∠ = 1.2°: Simmons, C. J.; Clearfield, A.; Sun, Y. *Inorg. Chim. Acta* **1986**, *121*, L3. (f) M = Cu, R = Ph, ∠ = 4.5°: Speier, G.; Fülöp, V. *J. Chem. Soc., Dalton Trans.* **1989**, 2331.

Table 7. Crystallographic Data for **1c**$(THF)_2$·2THF, [**1c**$(THF)_2]^+[BF_4]^-$, and **1c**$(CH_3CN)_2$·$3CH_3CN$

	1c$(THF)_2$·2THF	[**1c**$(THF)_2]^+[BF_4]^-$	**1c**$(CH_3CN)_2$·$3CH_3CN$
formula	$Ru_2C_{48}H_{60}O_{12}$	$Ru_2C_{40}H_{42}O_{10}BF_4$	$Ru_2C_{42}H_{43}N_5O_8$
color	deep red	orange	red
crystal dimens (mm)	0.16 × 0.32 × 0.40	0.25 × 0.25 × 0.35	0.20 × 0.36 × 0.36
space group	$P\bar{1}$	*C*2/*m*	*C*2/*c*
T (°C)	−154	−172	−169
a (Å)	10.730(5) Å	13.056(4) Å	27.058(3)
b (Å)	12.335(6)	21.358(6)	10.049(1)
c (Å)	9.193(4)	9.199(2)	17.956(2)
α (deg)	105.15(2)		
β (deg)	109.35(2)	111.28(1)	120.89(1)
γ (deg)	77.98(2)		
Z (molecules/cell)	2[a]	2	4
V (Å^3)	1098.20	2390.10	4190.04
calcd density (g/cm^3)	1.559	1.350	1.465
wavelength (Å)	0.710 69	0.710 69	0.710 69
mol wt	515.57[a]	971.71	923.95
linear abs coeff (cm^{-1})	7.353	6.798	7.588
detector to sample dist (cm)	22.5	22.5	22.5
sample to source dist (cm)	23.5	23.5	23.5
scan speed (deg/min)	4.0	10.0	8.0
scan width (deg + dispersion)	2.5	2.0	2.0
individual background (s)	6	4	4
2*θ* range (deg)	6−45	6−45	6−55
tot. no. of reflns collected	5931	2005	6504
no. of unique intensities	2892	1605	4826
no. with $F > 0.0$	2804	1522	4711
no. with $F > 3.0\sigma(F)$	2657		4535
no. with $F > 2.33\sigma(F)$		1329	
R for averaging	0.024	0.013	0.039
R(*F*)	0.0246	0.0395	0.0698
$R_w(F)$	0.0255	0.0431	0.0788
goodness of Fit for the last cycle	1.002	1.436	2.520
max Δ/σ for last cycle	0.001 for non-H 0.26 for H	0.11	0.005

[a] For $Z = 2$, the asymmetric unit contains $RuC_{24}H_{30}O_6$.

electron spin density in the *δ* orbital (**VI**). In the previously structured $M_2(O_2CAr)_4$ compounds,[48,49] the orientation of the ring depends on electronics and sterics, the former favoring a planar and the latter a perpendicular arrangement. In $Ru_2(O_2CAr)_4$ complexes however, the molecular orbital **V** may shift the balance toward a perpendicular arrangement, without introducing *ortho*-substituents.

The X-ray structures reported here show that the aromatic rings are essentially parallel to the carboxylate planes. This corresponds to structures already reported for $Ru_2(O_2CAr)_4^{n+}$ systems where Ar = C_6H_5 and $n = 0$, 1[6b] and Ar = *p*-C_6H_4-OMe and $n = 1$,[6a] suggesting that the solid-state orientation is not significantly affected by the aryl group, the axial ligand, or charge and that the electronic contributions still favor the parallel arrangement.

(a) X-ray Structures of $Ru_2(O_2C$-*p*-$C_6H_4CH_3)_4(THF)_2$ (1c-$(THF)_2$) and $[Ru_2(O_2C$-*p*-$C_6H_4CH_3)_4(THF)_2]^+[BF_4]^-$ ([1c-$(THF)_2]^+[BF_4]^-$). Up to this point, comparison of $Ru_2(O_2CR)_4^{n+}$ ($n = 0$, 1) species has been limited to species containing not only different charges but also different axial or equatorial ligands. Here we report the structures of neutral and cationic diruthenium tetracarboxylates which contain the same carboxylate groups and axial ligands. Crystallographic data are given in Table 7, selected bond distances and angles are presented in Tables 8 and 9, and ORTEP drawings are shown in Figures 11 and 12.[50]

Table 8. Selected Bond Distances (Å) and Bond Angles (deg) for **1c**$(THF)_2$·2THF

Distances			
Ru(1)−Ru(1)′	2.2689(11)	O(2)−C(3)	1.266(4)
Ru(1)−O(2)	2.0702(22)	O(4)−C(3)	1.276(4)
Ru(1)−O(4)	2.0570(22)	O(12)−C(13)	1.266(4)
Ru(1)−O(12)	2.0578(22)	O(14)−C(13)	1.275(4)
Ru(1)−O(14)	2.0692(22)	C(3)−C(5)	1.489(4)
Ru(1)−O(22)	2.3696(24)	C(13)−C(15)	1.482(4)
Angles			
Ru(1)′−Ru(1)−O(2)	90.47(7)	Ru(1)′−Ru(1)−O(14)	89.55(7)
Ru(1)′−Ru(1)−O(4)	88.83(7)	Ru(1)′−Ru(1)−O(22)	173.59(5)
Ru(1)′−Ru(1)−O(12)	89.75(7)		

Table 9. Selected Bond Distances (Å) and Bond Angles (deg) for [**1c**$(THF)_2]^+[BF_4]^-$

Distances			
Ru(1)−Ru(1)′	2.2618(16)	O(2)−C(3)	1.274(6)
Ru(1)−O(2)	2.013(3)	O(4)−C(3)	1.271(6)
Ru(1)−O(4)	2.107(4)	C(3)−C(5)	1.478(8)
Ru(1)−O(12)	2.258(6)		
Angles			
Ru(1)−Ru(1)′−O(2)	89.69(12)	Ru(1)−Ru(1)′−O(12)	178.025(16)
Ru(1)−Ru(1)′−O(4)	89.54(11)		

(49) (a) M = Cr, R = 2-C_6H_5Ph, ∠ = 45°: Cotton, F. A.; Thompson, J. L. *Inorg. Chem.* **1981**, *20*, 1292. (b) M = Mo, R = 2-C_6H_5Ph, ∠ = 48°: Cotton, F. A.; Thompson, J. L. *Inorg. Chem.* **1981**, *20*, 3887. (c) M = W, R = 2,4,6-Me_3Ph, ∠ = 42°: ref 48c. (d) M = Rh, R = 2-PhC_6H_5, ∠ = 74°: Cotton, F. A.; Thompson, J. L. *Inorg. Chim. Acta* **1984**, *81*, 193. (e) M = Cu, R = 2,6-MeO-Ph, ∠ = 58°: Erre, L. S.; Micera, G.; Piu, P.; Cariati, F.; Ciani, G. *Inorg. Chem.* **1985**, *24*, 2297.

(50) As noted in the Experimental Section, the full-matrix least-squares calculations of [**1c**$(THF)_2]^+[BF_4]^-$ did not allow the exact [**1c**$]^+$:$[BF_4]^-$ ratio to be determined. However, on the basis of the method of preparation and IR and NMR characterization, a 1:1 ratio was assumed. Comparison of the structural data with those for **1c**$(THF)_2$ also gave no indication that both cationic and neutral $Ru_2(O_2CR)_4$ units were present in the crystal.

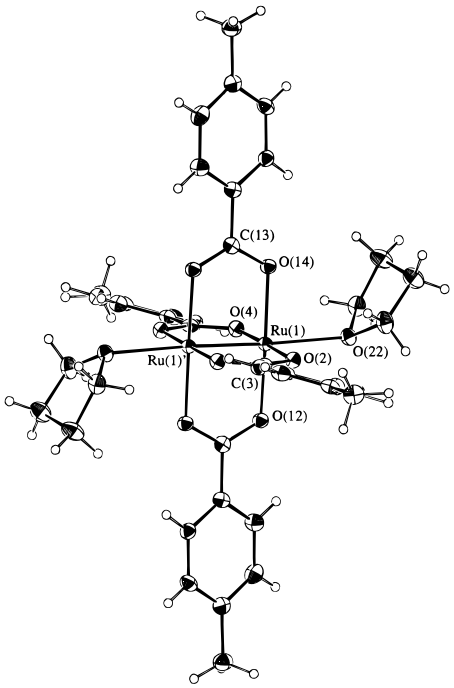

Figure 11. ORTEP drawing of $Ru_2(O_2C\text{-}p\text{-}C_6H_4CH_3)_4(THF)_2$.

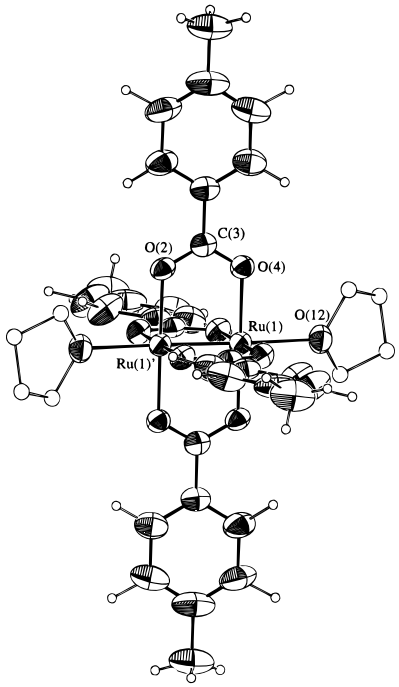

Figure 12. ORTEP drawing of $[Ru_2(O_2C\text{-}p\text{-}C_6H_4CH_3)_4(THF)_2]^+[BF_4]^-$ showing only one set of partially-occupied THF sites.

The primary difference between the two species, the charge of the core, did not affect the Ru−Ru bond distance. A distance of 2.2689(11) Å for **1c**$(THF)_2$ with four antibonding electrons compared with a distance of 2.2618(16) Å for $[\mathbf{1c}(THF)_2]^+[BF_4]^-$ with only three antibonding electrons supported the conclusion made by Cotton et al.[5d] that the additional electron in $Ru_2(O_2CR)_4$ must occupy the δ^*, rather than the π^*, orbital. Increased occupation of the π^* orbital, which is more antibonding, to give the electron configuration $\delta^{*1}\pi^{*3}$ would have significantly lengthened the Ru−Ru bond.

The identity of the axial ligand in the cationic species does affect the Ru−Ru bond, however. The Ru−Ru distance in $[\mathbf{1c}(THF)_2]^+[BF_4]^-$ is comparable to the Ru−Ru distance of 2.265(2) Å in $Ru_2(O_2CC_6H_5)_4(C_2H_5OH)_2^+$.[4h] Both distances are ca. 0.015 Å longer than the Ru−Ru distance of 2.248(1) Å in $Ru_2(O_2CCH_3)_4(H_2O)_2^+$ [4b] and are up to 0.03 Å shorter than the Ru−Ru distances (2.267−2.290 Å) in the reported $Ru_2(O_2CR)_4^+$ species with Cl^- coordinated in the axial position.[4b,h,i]

Both the Ru−O and Ru−O(THF) distances in $[\mathbf{1c}(THF)_2]^+[BF_4]^-$ (2.015 (average) and 2.258(6) Å, respectively) were shorter than those for **1c**$(THF)_2$ (2.064 (average) and 2.3696(24) Å, respectively). This was attributed to the contraction of the Ru d orbitals with the increased charge. Similar Ru−O distances are reported for other structurally-characterized $Ru_2(O_2CR)_4^+$ cores.[4b,h,i]

The dihedral angles between the carboxylate plane and the aromatic ring do vary between the neutral and cationic compounds, but both are essentially planar. For **1c**$(THF)_2$, the angles are 16.6 and 13.8°. For $[\mathbf{1c}(THF)_2]^+[BF_4]^-$, they are 7.3°. This difference can be simply attributed to lattice packing forces. Recall that the lattice of $[\mathbf{1c}(THF)_2]^+[BF_4]^-$ contains the BF_4^- counterion, while the lattice of **1c**$(THF)_2$ contains an additional 2 equiv of THF.

(b) X-ray Structure of $Ru_2(O_2C\text{-}p\text{-}C_6H_4CH_3)_4(CH_3CN)_2$ (1c$(CH_3CN)_2$). This structure, the first reported for a neutral diruthenium tetracarboxylate with nitrogen-containing axial ligands and potential π-acceptor ligands, contains a Ru_2^{4+} core essentially unaffected by the change in axial ligand. Crystallographic data are given in Table 7, selected bond distances and angles are presented in Table 10, and an ORTEP drawing is shown in Figure 13. Comparison to the bis-THF adduct (Table 8, Figure 11) shows that, despite enhanced axial ligand interactions, the Ru−Ru distance is insignificantly lengthened in the acetonitrile adduct. The Ru−N distance (2.331(5) Å) is shorter than the Ru−O(THF) distance (2.3696(24) Å). The Ru−Ru distance of 2.2757(10) Å is still within 3σ of that in the THF adduct (2.2689(11) Å). This suggests that no significant π-interactions occur. The Ru−Ru bond is not shortened, as would be expected should back-bonding from the Ru−Ru π^* into the acetonitrile π^* orbitals occur. Nor is the N≡C distance (1.144(9) Å) lengthened from the N≡C distance seen for the acetonitrile molecules in the lattice (1.142(12) Å). The axial acetonitrile ligands are linear (N−C−C is 179.0(7)°) but not collinear with the Ru−Ru bond (Ru−N−C is 155.8°). The angle is much larger than those seen for other end-bound nitriles (168.4−180°).[51]

(c) ^{1}H NMR Spectra of Toluates and Benzoates. Although the solid state structures suggest that π-polarization must be occurring, free rotation of the aromatic rings in the arenecarboxylates in solution could still allow direct π-delocalization to occur. Therefore, the π-contributions to the isotropic shift of the equatorial carboxylates in $Ru_2(O_2CAr)_4^{n+}$ (Ar = C_6H_5,

Table 10. Selected Bond Distances (Å) and Bond Angles (deg) for **1c**$(CH_3CN)_2\cdot 3CH_3CN$

Distances

Ru(1)−Ru(1)′	2.2757(10)	O(4)−C(3)	1.288(7)
Ru(1)−O(2)	2.061(4)	O(12)−C(13)	1.270(8)
Ru(1)−O(4)′	2.066(4)	O(14)−C(13)	1.280(7)
Ru(1)−O(12)	2.056(4)	O(14)′−C(13)′	1.280(7)
Ru(1)−O(14)′	2.067(4)	N(22)−C(23)	1.144(9)
Ru(1)−N(22)	2.331(5)	C(23)−C(24)	1.454(9)
O(2)−C(3)	1.260(7)		

Angles

Ru(1)′−Ru(1)−O(2)	89.58(12)	Ru(1)′−Ru(1)−N(22)	172.70(15)
Ru(1)′−Ru(1)−O(4)	89.63(12)	Ru(1)−N(22)−C(23)	155.8(5)
Ru(1)′−Ru(1)−O(12)	89.08(12)	N(22)−C(23)−C(24)	179.0(7)
Ru(1)′−Ru(1)−O(14)	90.19(11)		

(51) Storhoff, B. N.; Lewis, H. C., Jr. *Coord. Chem. Rev.* **1977**, *23*, 1.

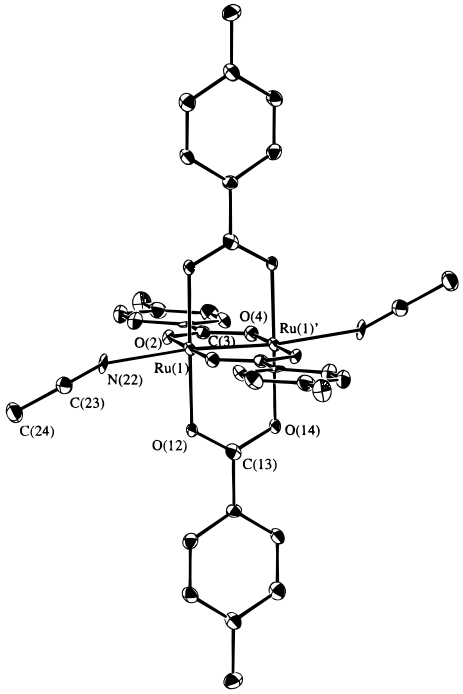

Figure 13. ORTEP drawing of $Ru_2(O_2C\text{-}p\text{-}C_6H_4CH_3)_4(CH_3CN)_2$.

Table 11. ^{1}H NMR Data and Isotropic Shifts[a] for $Ru_2(O_2CR)_4^{n+}$

	$Ru_2(O_2CR)_4$		$Ru_2(O_2CR)_4^+$	
	δ_{obs} (ppm)	δ_{iso} (ppm)	δ_{obs} (ppm)	δ_{iso} (ppm)
b: R = C_6H_5				
o-H	16.5	9.1	31.8	24.4
m-H	9.3	1.1	7.5	−0.7
p-H	10.7	3.3	19.7	12.3
c: R = *p*-$C_6H_4CH_3$				
o-H	16.4	9.2	31.7	24.5
m-H	9.1	1.3	7.4	−0.4
p-CH_3	2.9	0.6	−3.3	−5.6
d: R = $(CH_2)_2CH_3$				
CH_2(2)	2.9	0.1	−39	−42
CH_2(3)	7.4	5.6	15.6	13.8
CH_3(4)	6.3	5.4	11.1	10.2
e: R = $(CH)_2CH_3$				
CH(2)	7.0	0.5	−10.9[b]	−17.4
CH(3)	16.3	9.1	41.4[b]	34.2
CH_3(trans)	1.9	−0.3	−15.0[b]	−17.2
f: R = $(CH)C(CH_3)_2$				
CH(2)	4.7	−1.4	−18.4[c]	−24.5
CH_3(cis)	4.4	2.2	−5.4[c]	−7.6
CH_3(trans)	2.2	0.2	−12.8[c]	−14.7

[a] Calculated using eq 1 and $Mo_2(O_2CR)_4$ data. [b] T_1 (ms): CH(2), 7.11 ± 0.12; CH(3), 7.06 ± 0.09; CH_3(trans), 47 ± 1. [c] T_1 (ms): CH(2), 6.6 ± 0.7; CH_3(cis), 11 ± 1; CH_3(trans), 44 ± 2.

p-$C_6H_4CH_3$; $n = 0, 1$), were investigated. The solubility of these compounds, even in coordinating solvents, was slight. ^{1}H NMR spectra were taken in methanol-d_4/THF-d_8 mixtures, and the data are given in Table 11. Assignments of the proton signals were based on coupling patterns, relative intensities, and shifts upon methyl substitution. Isotropic shifts were calculated using the corresponding $Mo_2(O_2CR)_4$ chemical shifts as the diamagnetic shifts.

The solution isotropic shifts seen for the benzoate (**1b**) and toluate (**1c**) systems are not large, especially for the neutral systems, but do show an alternating downfield, upfield, downfield shift pattern for the *ortho*-, *meta*-, and *para*-protons, indicative of a π-contact mechanism.[27,38] The upfield shift seen upon substitution of the *para*-proton with a methyl group confirms the π-nature of the contact contribution.[27,38] For a system with π-delocalization, the shifts for the *ortho*-H and *para*-H should be comparable, which is not the case here (although the upfield dipolar contribution may diminish such an effect). Thus, the π-polarization mechanism appears to be occurring for the equatorial aromatic carboxylates, consistent with the planar arrangement seen in the solid state.

Table 12. Estimated Dipolar Shift Contributions[a] for *p*-Toluene Protons in **1c** and [**1c**]$^+$ with and without ZFS Terms

				δ_{dip} (ppm)		
		10^8r (cm)	θ (deg)	without ZFS[b]	with ZFS[c]	δ_{iso} (ppm)
1c	*o*-H	4.813	67.06	2.14	8.56	9.2
	m-H	6.921	74.59	1.04	4.16	1.3
	p-CH_3	8.819	86.08	0.63	2.51	0.6
[**1c**]$^+$	*o*-H	4.756	64.20	1.76	8.45	24.5
	m-H	7.074	71.92	0.88	4.23	−0.4
	p-CH_3	8.734	85.73	0.65	3.10	−5.6

[a] Calculated for 296 K. [b] Calculated using eq 3. [c] Calculated using eq 5 for **1c** and eq 6 for [**1c**]$^+$.

Table 13. Estimated Dipolar Shifts[a] for Axial THF Ligands

				δ_{dip} (ppm)		
		10^8r (cm)	θ (deg)	without ZFS[b]	with ZFS[c]	δ_{iso} (ppm)[d]
1	2-H	4.430	24.07	−10.5	−54.3	−19
	3-H	5.655	27.72	−4.55	−23.5	−15
[**1**]$^+$	2-H	4.304[e]	24.07	−11.5	−72.1	−29
	3-H	5.525[e]	27.72	−4.87	−30.7	−22

[a] Calculated for 213 K. [b] Calculated using eq 3. [c] Calculated using eq 5 for **1** and eq 6 for [**1**]$^+$. [d] From ^{1}H NMR spectra of **1a** and [**1a**]$^+$[BF_4]$^-$ and THF in toluene-d_8 at −58 °C. [e] Calculated using the X-ray data from **1c**, assuming a shortening of the Ru−O distance of 0.115 Å and no change in θ.

(d) Estimated Dipolar Shifts. Using the data from the crystal structures of **1c**$(THF)_2$ and **[1c**$(THF)_2]^+$[BF_4]$^-$, the dipolar shift contributions for equatorial toluate and axial THF ligands were estimated. Comparison of the observed and calculated values, with and without zero-field splitting contributions, for the equatorial toluate protons (Table 12) should indicate the relative importance of ZFS effects and the degree of contact contribution. For **1c**, the observed isotropic shift of the *ortho*-H, which is closest to the metal−metal bond, is in fairly good agreement with the value calculated with ZFS. The additional downfield shift can be attributed to π-contact contributions. For the *meta*-H and *para*-CH_3, the observed isotropic shifts are actually closer to the value calculated without ZFS. This, however, is likely an effect of the π-contributions, which should cause upfield shifts at both positions, cancelling out the downfield dipolar shift.

The calculations for the equatorial toluate protons in [**1c**$(THF)_2]^+$[BF_4]$^-$ ($S = {}^3/_2$) indicated that its dipolar contributions were not significantly increased over those of **1c**$(THF)_2$ ($S = 1$). When calculated using eq 3, which does not take ZFS into account, the dipolar shift values were actually slightly smaller due to the smaller $(g_{\parallel}^2 - g_{\perp}^2)$ term. The contribution from the ZFS term for [**1c**$(THF)_2]^+$[BF_4]$^-$ is comparable to that for **1c**$(THF)_2$, despite the higher S value, since the D value for the cationic compound is lower (75 cm^{-1} compared to 290 cm^{-1} for $S = 1$).[16,18] The difference between the calculated and observed values is again attributed to π-contact contributions, which, as concluded from the VT ^{1}H NMR data for **1a** and [**1a**]$^+$[X]$^-$, effectively dominate in the $S = {}^3/_2$ systems.

The X-ray data for the axial THF ligands in **1c**$(THF)_2$ were used to estimate its dipolar shift at −60 °C and compared to the ^{1}H NMR data for **1a** and [**1a**]$^+$[BF_4]$^-$ (Table 13). Here, it is apparent that ignoring ZFS does not predict sufficiently large

shifts. Inclusion of the ZFS term gives values significantly larger than the observed shifts for both **1a** and $[\mathbf{1a}]^+[BF_4]^-$ (by ~40 ppm for 2-H and 8 ppm for 3-H), suggesting that the proton resonances for the axial ligands are shifted downfield by a contact mechanism. This is consistent with the conclusion made from the ^{1}H NMR data for the axial carboxylate in $[\mathbf{1a}]^+$-$[O_2C(CH_2)_6CH_3]^-$. Since no evidence was seen for π-contributions with 2-MeTHF, a σ-contact mechanism must be occurring. Treating the system as two paramagnetic centers and calculating the dipolar shifts using the distance to the closest metal would only increase the dipolar estimate, confirming that placing the origin at the center of the metal−metal bond is a better model for the metal−metal multiply-bonded systems.

The Unsaturated Carboxylates. $Ru_2(O_2CR)_4^{n+}$ systems with C═C bonds in conjugation with the carboxylate group confirmed that π-contact contributions occur in the equatorial ligands. Comparison of the ^{1}H NMR chemical shifts of $Ru_2(O_2C(CH)_2CH_3)_4^{n+}$ (**1e**) and $Ru_2(O_2C(CH)C(CH_3)_2)_4^{n+}$ (**1f**), where $n = 0$, 1 (Table 11), showed that substitution of the CH-(3) proton with a methyl group affected all the proton signals, most likely due to geometry changes. Assignments were made using a combination of relative chemical shifts, intensity, coupling, T_1 measurements and isotropic shifts calculated using $Mo_2(O_2CR)_4$ chemical shifts. The upfield, downfield, upfield pattern seen for the crotonates is typical for π-contact contributions.[52] Substitution of the CH(3) in $Ru_2(O_2C(CH)_2CH_3)_4^+$, which gave a signal downfield at 41.4 ppm, with a methyl group shifted the signal upfield to −5.4 ppm, also indicative of π-contributions. Further evidence for a contact mechanism is seen when the isotropic shifts of the saturated butyrate (**1d**) and unsaturated crotonate (**1e**) are compared. A large shift from −42 ppm for the sp^3-hybridized CH_2(2) to −17.4 ppm for the sp^2-hybridized CH(2) occurs. The change in hybridization would not affect the dipolar shift significantly but would influence the hyperfine coupling (A_{con}), which determines the contact shift. Thus, evidence for contact shifts is seen for equatorial saturated, unsaturated, and arene carboxylates, the last two supporting a π-contact mechanism and the last, a π-polarization mechanism.

Conclusions

^{1}H NMR spectroscopy has proven to be a useful technique for studying paramagnetic $Ru_2(O_2CR)_4^{n+}$ species. Attempts to obtain a nonligated $Ru_2(O_2CR)_4$ species in noncoordinating solvents were unsuccessful. ^{1}H NMR, along with UV/visible, molecular weight, and electrochemical studies, indicated that **1a** and its diamagnetic Rh_2^{4+} analogue are oligomeric species with extended π-systems in noncoordinating solvents.

The axial geometry of the dimetal tetracarboxylate systems has allowed us to determine the factors contributing to the isotropic shifts of axial and equatorial ligands. The axial ligands are affected by both dipolar and contact shifts. Through-space interactions cause upfield shifts. One contact (through bonds) mechanism occurring with π-type ligands is direct π-delocalization, which suggests that $Ru_2(O_2CR)_4^{n+}$ units could be linked via their axial sites with bridging π-type ligands to form conductive polymers. Our investigation of this will be reported in a subsequent paper.[21] Comparison of the estimated dipolar shifts for axial THF ligands with observed chemical shifts suggests that downfield σ-contact contributions occur as well. The equatorial carboxylate ligands are also affected by both dipolar and contact shifts. In the long-alkyl-chain carboxylates the downfield dipolar shift dominates. In aromatic and conjugated systems, evidence for π-contact shifts is seen, the contact shift providing a major component of the isotropic shifts of the cationic species. Temperature dependence studies and calculations of the dipolar shifts show that zero-field splitting contributes significantly to the dipolar shift.

The similar ^{1}H NMR spectra seen for bis-adducts of **1a** with σ-donors (THF) and π-acceptors (pyrazine) and the similar Ru−Ru bond distances seen for $Ru_2(O_2C$-*p*-tolyl$)_4L_2$, where L = THF and CH_3CN, suggest that the π-acceptor ligands do not change the $\delta^{*2}\pi^{*2}$ ground state or significantly lower the $\delta^{*1}\pi^{*3}$ state. The solvent dependences of the electronic and Raman spectra of **1a** apparently reflect small electronic differences in π- and σ-interactions which combined have little effect on the Ru−Ru bond length.

Experimental Section

All ruthenium and molybdenum compounds were handled under argon or dinitrogen using Schlenk techniques and gloveboxes. Toluene, hexanes, THF, and diethyl ether were distilled from sodium or potassium with benzophenone, dichloromethane was distilled from calcium hydride under dinitrogen, and all were stored over molecule sieves. Methanol, acetonitrile, and diglyme were bought anhydrous from Aldrich and stored over molecular sieves. ^{1}H NMR spectra were recorded on a Varian XL-300 spectrometer, UV/visible spectra on a HP8452A diode array spectrophotometer with UV/visible operating software 89531A, and IR spectra on a Nicolet 510P FT-IR spectrophotometer using KBr disks. Elemental analyses were performed by Oneida Research Services.

$Ru_2(O_2CCH_3)_4$,[5b] $Ru_2(O_2CH)_4$,[5b] $Ru_2(O_2CCH_3)_4Cl$,[53] $Rh_2(O_2CCH_3)_4$,[54] and $Mo_2(O_2CR)_4$[55] were synthesized via literature methods. The carboxylic acids, pyrazine, 2,6-dimethylpyrazine, pyridine, 4-picoline, benzonitrile, $CrCl_2$, and $Mo(CO)_6$ were purchased from Aldrich and used without further purification.

Synthesis of $Ru_2(O_2CR)_4$ (1a−f). Method A. Toluene (200−250 mL) was added to $Ru_2(O_2CCH_3)_4$ or $Ru_2(O_2CH)_4$ (0.7 mmol) and the appropriate carboxylic acid (3.5 mmol) in a Schlenk flask equipped with a distillation arm. The mixture was refluxed for several hours, and most of the solvent was distilled off, removing the toluene/acetic acid or toluene/formic acid azeotrope. For R = $(CH_2)_6CH_3$ (**1a**), the solution was filtered and the toluene removed *in vacuo*. The brown residue was redissolved in methanol. **1a** was isolated as a brown precipitate. Yield: 45% from $Ru_2(O_2CH)_4$, 55−80% from $Ru_2(O_2CCH_3)_4$. Anal. Calcd for $Ru_2O_8C_{32}H_{60}$: C, 49.60; H, 7.80. Found: C, 49.55; H, 7.96. IR (cm^{-1}): 2959 s, 2924 s, 2851 s, 1545 vs, 1522 m, 1468 m, 1454 m, 1435 s, 1412 s, 1317 w, 1180 w, 1111 w, 723 m, 675 m, 478 w. Subsequent batches of precipitate contained $[\mathbf{1a}]^+$-$[O_2C(CH_2)_6CH_3]^-$. Anal. Calcd for $Ru_2O_{10}C_{40}H_{75}$: C, 52.23; H, 8.23. Found: C, 52.67; H, 8.84. IR (cm^{-1}): 2957 s, 2924 s, 2853 s, 1523 vs, 1493 s, 1456 vs, 1415 vs, 1317 w, 1107 m, 723 w, 667 m. For R = $(CH_2)_2CH_3$ (**1d**), the toluene solution was filtered and cooled to −20 °C. Precipitation generally yielded both **1d** and $[\mathbf{1d}]^+[O_2C(CH_2)_2CH_3]^-$. For R = C_6H_5 (**1b**), $C_6H_4CH_3$ (**1c**), $(CH)_2CH_3$ (**1e**), and $(CH)C(CH_3)_2$ (**1f**), the product, insoluble in toluene, was filtered off and washed with hexanes. **1b** and **1c** were recrystallized from THF; **1e** and **1f**, from methanol. IR for **1b** (cm^{-1}): 3094 w, 3065 w, 2964 m, 2878 w, 1595 m, 1549 s, 1495 w, 1175 w, 1157 w, 1070 m, 1042 m, 1028 m, 879 m, 845 m, 712 s, 689 m, 507 m. IR for **1c** (cm^{-1}): 3065 w, 3034 w, 2968 w, 2922 w, 2875 w, 1613 m, 1587 m, 1539 s, 1448 w, 1406 vs, 1293 w, 1178 m, 1143 w, 1020 m, 851 m, 838 m, 783 m, 754 s, 692 w, 636 m, 472 m. IR for **1e** (cm^{-1}): 3038 w, 2967 w, 2942 w, 2910 w, 2875 w, 2851 w, 1658 s, 1537 vs, 1498 m, 1445 m, 1415 vs, 1402 s, 1375 m, 1300 w, 1263 m, 1103 w, 966 m, 918 w, 841 w, 746 m, 688 w, 611 w, 488 w. IR for **1f** (cm^{-1}): 3034 w, 2970 w, 2930 w,

(52) Arafa, I. M.; Goff, H. M.; David, S. S.; Murch, B. P.; Que, L., Jr. *Inorg. Chem.* **1987**, *26*, 2779.

(53) (a) Marchon, J.-C.; Maldivi, P. Private communication. (b) Mitchell, R. W.; Spencer, A.; Wilkinson, G. *J. Chem. Soc., Dalton Trans.* **1973**, 846.

(54) Rempel, G. A.; Legzdins, P.; Smith, H.; Wilkinson, G. *Inorg. Synth.* **1972**, *13*, 90.

(55) Brignole, A. B.; Cotton, F. A. *Inorg. Synth.* **1972**, *13*, 81.

2912 w, 2856 w, 1647 s, 1528 vs, 1499 m, 1443 s, 1408 vs, 1369 m, 1313 s, 1186 m, 1076 m, 1023 m, 858 m, 763 m, 603 w, 495 w.

Method B.[14b] $Ru_2(O_2CR)_4Cl$ (0.63 mmol) was dissolved in a 1:1 MeOH/H_2O solvent mixture (20 mL). An aqueous solution of $CrCl_2$ (0.95 mmol in ca. 10 mL) was added. For R = $(CH)C(CH_3)_2$ (**1f**) and $(CH_2)_2CH_3$ (**1d**), the product precipitated immediately and was isolated by filtration. IR for **1d** (KBr, cm^{-1}): 2963 s, 2934 m, 2874 m, 1550 vs, 1522 s, 1462 s, 1431 s, 1419 s, 1346 w, 1315 m, 1263 m, 1213 w, 1103 m, 1047 w, 897 w, 870 w, 800 m, 737 m, 652 m, 582 w, 451 m, 435 m.

Method C. A Ru(II) blue solution[56] (2.2 g, 8.4 mmol) in methanol (20 mL) was added to $NaO_2C(CH_2)_6CH_3$ (5.6 g, 33.7 mmol) in methanol (50 mL), and the mixture was refluxed for 22 h. The solution turned from blue to green to brown with the formation of precipitate. After cooling of the mixture to room temperature, an unidentified black precipitate was filtered off and washed with methanol. Yield: 1.09 g. IR (cm^{-1}): 2957 s, 2924 s, 2855 s, 2811 m, 1936 w, 1732 w, 1522 vs, 1415 s, 1316 m, 1110 w, 1020 m, 551 m. ^1H NMR (benzene-d_6, δ): 0−2 ppm (vbr). UV/visible (benzene, λ_{max}): 342 nm. Upon cooling of the mixture to 10 °C, **1a** precipitated from the mother liquor. Yield: 1.56 g, 48%.

Synthesis of $Ru_2(O_2CR)_4Cl$ ([1a−f]$^+$[Cl]$^-$). Method A. $Ru_2(O_2CCH_3)_4Cl$ (1.6 mmol) was dissolved in hot methanol (40 mL). The appropriate carboxylic acid (7.2−8.0 mmol) was added and the solution stirred at 50 °C for several days. The solvent was removed and the residue checked by ^1H NMR. If acetate groups were still present, more carboxylic acid and methanol were added and the solution was stirred longer. For R = $(CH_2)_6CH_3$ ([**1a**]$^+$[Cl]$^-$), the final residue was dissolved in toluene. Addition of hexanes caused precipitation of [**1a**]$^+$[Cl]$^-$. Yield: 93%. IR (cm^{-1}): 2957 s, 2926 s, 2855 s, 1458 vs, 1431 vs, 1318 m, 725 w, 690 m, 679 m. For R = $(CH)_2CH_3$ ([**1e**]$^+$[Cl]$^-$), the final residue was dissolved in THF. Addition of hexanes caused precipitation of [**1e**]$^+$[Cl]$^-$. IR (cm^{-1}): 3047 w, 2969 w, 2942 w, 2913 w, 2855 w, 1653 s, 1416 vs, 1302 w, 1252 m, 1103 w, 1007 w, 965 m, 918 w, 839 w, 745 s, 696 w, 625 w, 509 m.

Method B.[53a] $Ru_2(O_2CCH_3)_4Cl$ (0.33 g) and $HO_2C(CH_2)_2CH_3$ (15 mL) were stirred at 170 °C. After all the solid had dissolved, the solution was cooled to 10 °C. The resulting precipitate was filtered off and washed with diethyl ether, yielding [**1d**]$^+$[Cl]$^-$ (0.298 g). IR (cm^{-1}): 2965 m, 2934 w, 2876 w, 1464 s, 1450 s, 1427 vs, 1329 m, 1265 m, 1211 m, 1097 m, 1020 w, 897 w, 808 m, 758 w, 736 w, 677 m, 459 m.

Method C.[57] $Ru_2(O_2CCH_3)_4Cl$ (0.075 g, 0.158 mmol) was dissolved in 20 mL of a 1:1 MeOH/H_2O mixture. The carboxylic acid (0.95 mmol) dissolved in methanol was added to the $Ru_2(O_2CCH_3)_4Cl$ solution. The reaction mixture was stirred at 90−95 °C for $2^1/_2$ h. The precipitate was filtered off and washed with diethyl ether. IR for R = C_6H_5 ([**1b**]$^+$[Cl]$^-$) (cm^{-1}): 3068 w, 3054 w, 1601 m, 1497 m, 1466 s, 1408 vs, 1176 w, 1026 m, 845 w, 716 m, 691 s, 530 m. IR for R = $C_6H_4CH_3$ ([**1c**]$^+$[Cl]$^-$) (cm^{-1}): 3039 w, 3013 w, 2965 w, 2919 w, 1611 m, 1514 w, 1451 m, 1408 vs, 1180 m, 1020 w, 783 w, 758 s, 642 m, 500 m. Yield: 0.090 g, 73%.

Synthesis of $Ru_2(O_2CR)_4BF_4$ ([1a−f]$^+$[BF_4]$^-$). Method A.[57] A solution of $AgBF_4$ (0.14 mmol) in THF (15 mL) was added to $Ru_2(O_2CR)_4Cl$ (0.10 mmol) in THF (30 mL). The reaction mixture was stirred for 12 h and filtered over Celite. Addition of hexanes to the THF solution resulted in a precipitate. For R = C_6H_5 ([**1b**]$^+$[BF_4]$^-$) and $C_6H_4CH_3$ ([**1c**]$^+$[BF_4]$^-$), cooling the solution to −20 °C resulted in the formation of crystals. IR for [**1b**]$^+$[BF_4]$^-$ (KBr, cm^{-1}): 3073 w, 2977 w, 2892 w, 1601 m, 1497 m, 1464 s, 1406 vs, 1181 w, 1143 w, 1057 s, 1024 s, 860 w, 845 w, 720 s, 690 s, 534 m. IR for [**1c**]$^+$[BF_4]$^-$ (cm^{-1}): 2967 w, 2922 w, 2894 w, 1607 m, 1514 m, 1449 m, 1406 vs, 1182 s, 1145 w, 1057 s, 1020 m, 854 w, 783 w, 758 s, 642 m, 500 m, 480 m, 457 w.

Method B. A solution of $AgBF_4$ (0.14 mmol) in THF (15 mL) added to $Ru_2(O_2CR)_4$ (0.10 mmol) and THF (30 mL) was worked up as in method A.

Synthesis of $Rh_2(O_2C(CH_2)_6CH_3)_4$ (3a). Method A. $Rh_2(O_2CCH_3)_4MeOH_2$ was treated as in method A for $Ru_2(O_2CR)_4$. The residue remaining after removal of toluene was redissolved in CH_3CN. The first batches of blue precipitate contained what is believed to be $Rh_2(O_2C(CH_2)_6CH_3)_5$. ^1H NMR (benzene-d_6), δ): 17 (vbr), 4.8 (br), 2.2, 1.4, 0.9. ^1H NMR (methanol-d_4, δ): 10 (br), 2.9 (br), 0.9, 0.6. IR (KBr, cm^{-1}): 2957 m, 2924 s, 2872 w, 2853 m, 1587 s, 1508 w, 1468 w, 1458 w, 1435 m, 1414 m. The subsequent batches of purple precipitate contained $Rh_2(O_2C(CH_2)_6CH_3)_4(CH_3CN)_2$. Drying *in vacuo* at 45 °C produced $Rh_2(O_2C(CH_2)_6CH_3)_4$. ^1H NMR (benzene-d_6, δ): 2.9 (br), 20 (br), 1.39, 0.95. ^1H NMR (methanol-d_4, δ): 3.2 (mult, 2H, CH_2(2)), 1.96 (t, 2H, CH_2(3)), 1.32 (quint, 2H, (CH_2(4)), 1.1 (mult, 4H, CH_2(5), CH_2(6)), 1.0 (mult, 2H, CH_2(7)), 0.77 (t, 3H, CH_3(8)). IR (cm^{-1}): 2957 m, 2924 s, 2872 w, 2851 m, 1568 vs, 1522 w, 1468 w, 1433 m, 1414 s, 1313 w, 738 w, 679 m.

Method B. A 25 mL portion of octanoic acid was added to $Rh_2(O_2CCH_3)_4(MeOH)_2$ (0.27 g). The reaction mixture was stirred at 70 °C overnight. Precipitate formed after standing at room temperature several days. After filtration and washing with hexane, the product was recrystallized from acetonitrile.

NMR Experiments. All ^1H NMR spectra of the $Ru_2(O_2CR)_4^{n+}$ species were referenced to the protio solvent signal (benzene-d_6, 7.15; toluene-d_8, 2.09; methanol-d_4, 4.78; THF-d_8, 3.58 ppm). Spectra were accumulated using shortened delay times of 0.8 s for $n = 1$ and 1.0 s for $n = 0$. T_1 times were measured by using the inversion recovery method and least-squares analysis available on the Varian XL-300. The available COSY and HETCOR routines were also used. Evans' method experiments[58] were performed on 10^{-3} M samples in 2% v/v tetramethylsilane solution. The toluene-d_8 solutions of **1a** gave μ_{eff} values of 2.84, 2.80, and 2.76 μ_B. THF-d_8 solutions gave values of 2.69 and 2.86 μ_B.

The ^1H NMR resonances for axial ligands with π-systems (pyrazine, 2,6-dimethylpyrazine, pyridine, 4-picoline) and without (THF and 2-methyltetrahydrofuran) (Table 2) were located by adding 2−5 equiv and 10 equiv, respectively, of the ligand to **1a** and [**1a**]$^+$[BF_4]$^-$ in toluene-d_8. To slow any exchange processes and allow comparison of the temperature-dependent chemical shifts, samples were cooled to −58 °C, except for 4-picoline and [**1a**]$^+$[BF_4]$^-$, which gelled at −40 °C. Interactions of benzonitrile with **1a** were studied using 6 equiv of benzonitrile.

The ^{13}C NMR resonances for the carbons closest to the diruthenium core in **1a** in both THF-d_8 and toluene-d_8 were broad and difficult to locate. Resonances in the 14−35 ppm range in THF-d_8 were assigned using a 2-D HETCOR experiment. ^{13}C NMR T_1 measurements confirmed these assignments and were used to assign the signals for **1a** in toluene-d_8 (Table 3).

^1H NMR Data for $Mo_2(O_2CR)_4$. For R = C_6H_5 (methanol-d_4/THF-d_8, δ): 7.4 (2H, *o*-H), 8.2 (2H, *m*-H), 7.4 (1H, *p*-H). For R = *p*-$C_6H_4CH_3$ (methanol-d_4/THF-d_8, δ): 7.2 (2H, *o*-H), 7.8 (2H, *m*-H), 2.3 (3H, *p*-CH_3). For R = $(CH_2)_2CH_3$ (methanol-d_4, δ): 2.8 (2H, CH_2(2)), 1.8 (2H, CH_2(3)), 0.9 (3H, CH_3(4)). For R = $(CH)_2CH_3$ (methanol-d_4/THF-d_8, δ): 6.5 (1H, CH(2)), 7.2 (1H, CH(3)), 2.2 (3H, CH_3(trans)). For R = $(CH)C(CH_3)_2$ (methanol-d_4/THF-d_8, δ): 6.1 (1H, CH(2)), 2.2 (3H, CH_3(cis)), 1.9 (3H, CH_3(trans)).

^{13}C NMR Data for $Mo_2(O_2C(CH_2)_6CH_3)_4$. In toluene-d_8 at 61 °C (δ, T_1 (s)): 185.4 (C(1), 8.2 ± 0.3), 37.3 (C(2), 0.66 ± 0.04), 27.3 (C(3), 1.13 ± 0.03), 29.7 (C(4), 1.5 ± 0.1), 29.6 (C(5), 2.5 ± 0.1), 32.4 (C(6), 3.4 ± 0.1), 23.1 (C(7), 5.4 ± 0.4), 14.2 (C(8), 6.8 ± 0.3). In THF-d_8 at 61 °C (δ, T_1 (s)): 184.9 (C(1), 20 ± 1), 37.6 (C(2), 1.29 ± 0.03), 27.7 (C(3), 1.6 ± 0.1), 30.1 (C(4), 2.3 ± 0.1), 30.0 (C(5), 3.3 ± 0.1), 32.8 (C(6), 4.8 ± 0.1), 23.5 (C(7), 6.0 ± 0.2), 14.3 (C(8), 7.2 ± 0.3).

Solution Molecular Weight Measurements. Measurements were performed under argon in freshly-distilled, degassed benzene using cryoscopic equipment assembled in-house. Solutions were cooled in an air-jacketed glass apparatus immersed in an ice bath. Changes in temperature were monitored using a thermistor which plotted resistivity on a chart recorder. The system was calibrated by using freshly-sublimed biphenyl.

(56) (a) Rose, D.; Wilkinson, G. *J. Chem. Soc. A* **1970**, 1791. (b) Gilbert, J. D.; Rose, D.; Wilkinson, G. *J. Chem. Soc. A* **1970**, 2765.
(57) Barral, M. C.; Jiménez-Aparicio, R.; Rial, C.; Royer, E.; Saucedo, M. J.; Urbanos, F. A. *Polyhedron* **1990**, *9*, 1723.
(58) Evans, D. F. *J. Chem. Soc.* **1959**, 2003.

Table 14. Atomic Coordinates and Isotropic Thermal Parameters for $Ru_2(O_2C\text{-}p\text{-}C_6H_4CH_3)_4(THF)_2\cdot 2THF$

atom	10^4x	10^4y	10^4z	$10B_{iso}$ (Å^2)
Ru(1)	692.9(2)	356.5(2)	1188.8(3)	11
O(2)	233(2)	−480(2)	454(2)	14
C(3)	2113(3)	−1075(3)	−933(4)	14
O(4)	−951(2)	1200(2)	1881(2)	14
C(5)	3263(3)	−1657(3)	−1533(4)	14
C(6)	3077(3)	−2473(3)	−2914(4)	16
C(7)	4139(3)	−2997(3)	−3497(4)	17
C(8)	5416(3)	−2701(3)	−2727(4)	16
C(9)	5587(3)	−1875(3)	−1352(4)	17
C(10)	4538(3)	−1370(3)	−750(4)	16
C(11)	6558(4)	−3271(3)	−3360(5)	21
O(12)	765(2)	1724(2)	344(2)	15
C(13)	64(3)	1798(3)	−1047(4)	14
O(14)	645(2)	−1048(2)	1993(2)	14
C(15)	70(3)	2825(3)	−1595(4)	15
C(16)	−911(3)	3127(3)	−2910(4)	16
C(17)	−909(3)	4107(3)	−3371(4)	17
C(18)	75(3)	4808(3)	−2564(4)	17
C(19)	1066(4)	4479(3)	−1273(4)	21
C(20)	1051(3)	3524(3)	−783(4)	19
C(21)	80(4)	5876(3)	−3047(5)	22
O(22)	1958(2)	1076(2)	3798(2)	16
C(23)	3250(3)	438(3)	4345(4)	19
C(24)	3121(4)	−137(3)	5519(5)	25
C(25)	2196(4)	726(3)	6310(5)	24
C(26)	1299(4)	1323(4)	5029(4)	22
O(27)	4138(3)	−5561(2)	−2353(3)	34
C(28)	4033(4)	−6724(3)	−2472(5)	30
C(29)	5541(4)	−5443(3)	−1807(5)	28
C(30)	6270(4)	−6511(3)	−1267(5)	27
C(31)	5387(14)	−7368(3)	−2397(5)	26

Cyclic Voltammetry. Cyclic voltammograms were run using an EG&G Model 273A potentiostat/galvanostat and Model 270 Electrochemical Analysis Software 3.00. A platinum disk working electrode, a platinum wire auxiliary electrode, and an Ag/AgCl reference electrode were used. Sample solutions were ca. 1×10^{-3} M in 0.1 M $^nBu_4NPF_6$ electrolyte. $E_{1/2}$ values were referenced to the ferrocene/ferrocinium couple.

Samples of $M_2(O_2C(CH_2)_6CH_3)_4$ scanned at 100 mV/s gave the following data. In CH_2Cl_2: M = Ru, $E_a - E_c = 135.5$ mV, $E_{1/2} = 192$ mV, $E_{1/2(cor)} = -233$ mV; M = Rh, $E_a = E_c = 250$ mV, $E_{1/2} = 1245$ mV, $E_{1/2(cor)} = 820$ mV; M = Mo, $E_a - E_c = 95.4$ mV, $E_{1/2} = 552$ mV, $E_{1/2(cor)} = 152$ mV. In THF: M = Ru, $E_a - E_c = 97.5$ mV, $E_{1/2} = 177$ mV, $E_{1/2(cor)} = -369$ mV; M = Mo, $E_a - E_c = 99.5$ mV, $E_{1/2} = 466$ mV, $E_{1/2(cor)} = -80$ mV. In CH_3CN: M = Ru, $E_a - E_c = 83.0$ mV, $E_{1/2} = 94$ mV, $E_{1/2(cor)} = -292$ mV; M = Rh, $E_a - E_c = 164$ mV, $E_{1/2} = 1122$ mV, $E_{1/2(cor)} = 736$ mV; M = Mo, $E_a - E_c = 103.5$ mV, $E_{1/2} = 372$ mV, $E_{1/2(cor)} = -14$ mV.

Resonance Raman Studies. Excitation was provided by the 514.5 nm line of an Ar ion laser (Spectra Physics Model 2025). To minimize photodegradation, samples were spun at a rate of 50 rpm and laser power was kept below 100 mW. Scattered light was focused into a Jobin Yvon Mole S3000 triple monochromator (slits set to 3−4 cm^{-1} resolution). Samples were prepared in an inert-atmosphere glovebox and flame-sealed in 5 mm NMR tubes upon removal.

X-ray Structure Determinations. General operating procedures and listings of programs used have been previously reported.[59] A summary of the crystallographic data is given in Table 7. Data were collected using a standard moving-crystal, moving-detector technique. Data were corrected for Lorentz and polarization terms, and equivalent data were averaged. Structures were solved by direct methods (MULTAN78) and Fourier techniques. Atomic coordinates are given in Tables 14−16.

(a) $Ru_2(O_2C\text{-}p\text{-}C_6H_4CH_3)_4(THF)_2\cdot 2THF$. Data were collected at −154 °C. Due to broad Ω scans, the scan width was chosen to be 2.5°. Unit cell dimensions were determined by a least-squares fit of the setting angles for 50 carefully centered reflections having 2θ values between 24 and 32°. No correction for absorption was carried out. Plots of four standard reflections measured every 300 reflections showed no significant trends.

Following the initial refinement, all of the hydrogen atoms were located. The full-matrix least-squares refinement was completed by using anisotropic thermal parameters on the non-hydrogen atoms and isotropic thermal parameters on the hydrogen atoms. The final $R(F)$ was 0.0246. All reflections were included. Reflections having $F < 3.0\sigma(F)$ were given zero weight. The total number of variables was 401, including the scale factor and an overall isotropic extinction parameter. The final difference map was essentially featureless, the largest peak being 0.46 e/Å^3 in the vicinity of the Ru atom and the largest hole being −0.35 e/Å^3.

(59) Chisholm, M. H.; Folting, K.; Huffman, J. C.; Kirkpatrick, C. C. *Inorg. Chem.* **1984**, *23*, 1021.

Table 15. Atomic Coordinates and Isotropic Thermal Parameters for $Ru_2(O_2C\text{-}p\text{-}C_6H_4CH_3)_4(NCCH_3)_2\cdot 3CH_3CN$

atom	10^4x	10^4y	10^4z	$10B_{iso}$ (Å^2)
Ru(1)	4817.8(2)	673.1(5)	5310.8(3)	10
O(2)	4083(2)	9525(4)	4770(3)	9
C(3)	5953(3)	1472(6)	5680(4)	11
O(4)	5555(2)	1820(4)	5833(3)	11
C(5)	6484(3)	2319(6)	6064(4)	11
C(6)	6530(3)	3431(7)	6536(4)	14
C(7)	7020(3)	4239(7)	6894(4)	17
C(8)	7475(3)	3912(7)	6771(4)	17
C(9)	7429(3)	2773(6)	6293(4)	15
C(10)	6943(3)	1987(6)	5948(4)	12
C(11)	8008(3)	4762(7)	7148(5)	19
O(12)	5206(2)	9491(4)	6399(3)	11
C(13)	5489(3)	8474(6)	6412(4)	13
O(14)	4440(2)	1860(4)	4215(3)	10
C(15)	5767(3)	7635(6)	7208(4)	12
C(16)	5719(3)	7959(6)	7924(4)	14
C(17)	5957(3)	7177(6)	8644(4)	15
C(18)	6247(3)	6010(7)	8687(4)	16
C(19)	6308(3)	5698(6)	7982(4)	16
C(20)	6068(3)	6499(6)	7253(4)	13
C(21)	6491(3)	5075(7)	9467(5)	20
N(22)	4463(2)	1826(5)	6065(4)	14
C(23)	4313(3)	1951(6)	6551(4)	14
C(24)	4123(3)	2136(7)	7169(5)	21
C(25)	3111(4)	2240(8)	4109(5)	27
C(26)	3012(3)	1583(7)	2748(5)	23
N(27)	2937(4)	1071(9)	5250(6)	40
C(28)	4912(6)	4900(16)	5323(9)	68(3)
C(29)	4897(11)	4650(25)	6039(16)	48(5)

Table 16. Atomic Coordinates and Isotropic Thermal Parameters for $[Ru_2(O_2C\text{-}p\text{-}C_6H_4CH_3)_4(THF)_2]^+[BF_4]^-$

atom	10^4x	10^4y	10^4z	$10B_{iso}$ (Å^2)
Ru(1)	4380(1)	5000	8764(1)	29
O(2)	3514(3)	5666(2)	9359(5)	34
C(3)	3868(4)	5873(2)	10754(7)	34
O(4)	5260(3)	5670(2)	8200(4)	34
C(5)	3225(5)	6366(2)	11163(7)	38
C(6)	2207(5)	6546(3)	10088(10)	56
C(7)	1602(6)	7009(3)	10488(11)	65
C(8)	2013(7)	7296(3)	11938(12)	63
C(9)	3044(7)	7118(3)	12990(9)	59
C(10)	3642(5)	6655(3)	12606(8)	49
C(11)	1371(7)	7795(3)	12370(11)	72
O(12)	3185(5)	5000	6270(7)	41
C(13)	2553(14)	4490(7)	5616(17)	70
C(14)	2959(11)	5000	3644(15)	39
C(15)	2152(13)	4598(7)	3903(15)	93
C(16)	3343(14)	4587(8)	5050(16)	71
O(17)	740(17)	5000	9534(29)	105
C(18)	0	4447(6)	10000	93
C(19)	314(16)	5377(10)	8764(26)	90
B(20)	10000	3601(13)	5000	46
F(21)	9003(11)	3386(6)	5037(19)	94
F(22)	9705(17)	4154(8)	4139(19)	146
F(23)	9364(18)	3613(10)	3700(20)	153
F(24)	10265(21)	3330(17)	4090(36)	249

(b) $[Ru_2(O_2C\text{-}p\text{-}C_6H_4CH_3)_4(THF)_2]^+[BF_4]^-$. Data were collected at −172 °C. Unit cell dimensions were determined using 32 reflections. The ruthenium atom and toluate ligands were easily located, but the THF and BF_4 moieties were badly disordered. In spite of the disorder, a difference Fourier map phased on the non-hydrogen atoms clearly located all hydrogen atoms (except those on the THF), and these were included in subsequent least-squares refinement. The exact stoichiometry of the sample could not be confirmed on the basis of crystallographic data, since the full-matrix least-squares refinement did not rule out partial occupancy of the BF_4 site. A final difference Fourier map was essentially featureless, the largest peak being 0.21 e/Å^3.

(c) $Ru_2(O_2C\text{-}p\text{-}C_6H_4CH_3)_4(CH_3CN)_2\cdot 3CH_3CN$. Data were collected at −169 °C. Unit cell dimensions were determined by a least-squares fit of the setting angles for 50 carefully centered reflections having 2θ values between 24 and 33°. No correction for absorption was carried out. Plots of four standard reflections measured every 300 reflections showed no significant trends.

Following the initial refinement, many of the hydrogen atoms were evident in a differential Fourier map. Hydrogen atoms were introduced in fixed idealized positions and the full-matrix least-squares refinement was completed by using anisotropic thermal parameters on the non-hydrogen atoms. The final $R(F)$ was 0.070 using the full unique data. Reflections having $F < 3.0\sigma(F)$ were given zero weight. The total number of variables was 253, including the scale factor and an overall isotropic extinction parameter. The final difference map was essentially featureless, the largest peak being 1.0 e/Å^3 in the vicinity of C(28) (in a solvent molecule) and the largest hole being −1.1 e/Å^3.

Acknowledgment. We thank the National Science Foundation for support of this work. We also thank Johnson Matthey for a generous loan of ruthenium trichloride, L. Zollars for assisting with the 2-D NMR experiments, Professor D. W. Margerum and L. Schurter for use of their near-IR spectrophotometer at Purdue University, and M. Wemple and H. Eppley for helpful discussions.

Supporting Information Available: Complete listings of bond distances and angles, tables of anisotropic thermal parameters, and VERSORT drawings with complete atom number schemes for $Ru_2(O_2C\text{-}p\text{-}C_6H_4CH_3)_4(THF)_2\cdot 2THF$, $Ru_2(O_2C\text{-}p\text{-}C_6H_4CH_3)_4(CH_3CN)_2\cdot 3CH_3CN$, and $[Ru_2(O_2C\text{-}p\text{-}C_6H_4CH_3)_4(THF)_2]^+[BF_4]^-$ and calculations of dipolar shift sign changes (23 pages). Ordering information is given on any current masthead page.

IC950860U